UCRL-10717

University of California

Ernest O. Lawrence Radiation Laboratory

TWO-WEEK LOAN COPY

This is a Library Circulating Copy which may be borrowed for two weeks. For a personal retention copy, call Tech. Info. Division, Ext. 5545

LIQUID-LIQUID INTERFACIAL-TENSION MEASUREMENT WITH AN OSCILLATING JET

Berkeley, California

DISCLAIMER

This document was prepared as an account of work sponsored by the United States Government. While this document is believed to contain correct information, neither the United States Government nor any agency thereof, nor the Regents of the University of California, nor any of their employees, makes any warranty, express or implied, or assumes any legal responsibility for the accuracy, completeness, or usefulness of any information, apparatus, product, or process disclosed, or represents that its use would not infringe privately owned rights. Reference herein to any specific commercial product, process, or service by its trade name, trademark, manufacturer, or otherwise, does not necessarily constitute or imply its endorsement, recommendation, or favoring by the United States Government or any agency thereof, or the Regents of the University of California. The views and opinions of authors expressed herein do not necessarily state or reflect those of the United States Government or any agency thereof or the Regents of the University of California.

This report submitted also as
a Ph. D. Thesis by

Alfred E. Vandegrift

UCRL-10717
Chemistry UC-4
TID-4500 (19th Ed.)

UNIVERSITY OF CALIFORNIA

Lawrence Radiation Laboratory
Berkeley, California

Contract No. W-7405-eng-48

LIQUID-LIQUID INTERFACIAL-TENSION MEASUREMENT WITH AN OSCILLATING JET

Alfred E. Vandegrift, Peter N. Tenney,
and Theodore Vermeulen

March 11, 1963

Printed in USA. Price $2.25. Available from the
Office of Technical Services
U. S. Department of Commerce
Washington 25, D.C.

LIQUID-LIQUID INTERFACIAL-TENSION MEASUREMENT WITH AN OSCILLATING JET

Contents

Abstract v

I. Introduction 1

II. Statement of the Problem 5

III. Mathematical Study 6

A. Introduction 6

B. Liquid-Liquid Oscillating Jet 8

C. Velocity Profile of a Cylindrical Immiscible Liquid-Liquid Jet . . . 28

IV. Experimental Study 48

A. Apparatus and Measurements 48

B. Materials 48

C. Physical Properties 48

D. Optics 51

E. Preparation of Nozzles 55

F. Measurements 57

V. Discussion 60

VI. Conclusions 66

Acknowledgment 67

Nomenclature 68

Appendixes

Appendix A. Experimental Data 71

Appendix B. Computer Programs 80

References 97

LIQUID-LIQUID INTERFACIAL-TENSION MEASUREMENT WITH AN OSCILLATING JET

Alfred E. Vandegrift, Peter N. Tenney,
and Theodore Vermeulen

Lawrence Radiation Laboratory and
Department of Chemical Engineering
University of California
Berkeley, California

March 11, 1963

ABSTRACT

In this study the oscillating-jet technique, which has been used for some time to measure both the static and dynamic surface tension between a gas and a liquid, has been extended to the measurement of the interfacial tension between two immiscible liquids. The one previous study done on liquid-liquid systems was entirely experimental and empirical. In the present application, both a theory and new experimental techniques have been developed. This work was undertaken in order to obtain a method of studying interfacial concentrations in liquid-liquid systems undergoing mass transfer; progress has been made toward this goal, and recommendations are made for the next phase of this project.

The mathematical derivation given here is an extension of Bohr's theory for the gas-liquid case. However, since this theoretical treatment required as its input the velocity profile of the oscillating jet, an average profile has been solved for in the case of a circular liquid-liquid jet, as a second theoretical problem. The extension of Bohr's mathematics with the incorporated velocity profile gives a mathematical expression that calculates the interfacial tension to within 25% of the actual value in most cases; a large part of the observed deviation is believed to be experimental.

Data have been taken on immiscible-liquid pairs whose interfacial tension ranges from 6 to 42 dyn/cm. Experimental techniques are described for preparing the elliptical nozzles, illuminating the jet properly, and measuring the wavelength of oscillation. It has been found that the best methods for preparing nozzles for liquid-gas systems

do not give the best nozzles for liquid-liquid systems. The lighting and measuring techniques are different from those used in liquid-gas systems, because of the different range of refractive-index ratio in two-liquid systems.

I. INTRODUCTION

When a jet of liquid is forced through an elliptical orifice under a constant pressure, a standing wave is formed by the oscillations of the issuing stream about its equilibrium cylindrical form. The standing-wave pattern formed by the stream is the basis for an experimental method of obtaining the surface tension between a liquid and a gas, or the interfacial tension between two immiscible liquids.

The ultimate aim of the project is to study interfacial concentration while mass transfer is occurring. This will be possible because as a solute is transferred to the interface—and through it—the interfacial tension will change; this change can be followed by the change in wavelength of the jet. The concentration is related to the interfacial tension by the Gibbs adsorption isotherm.

A jet is particularly suitable for mass-transfer studies because its area and residence time can be determined accurately. Also, it can be caught at a variable distance from the nozzle, and analyzed chemically to give the mass-transfer rate as a function of length. Knowledge of how the interfacial concentration varies during mass transfer between two liquids should give a clearer understanding of the fundamental processes involved.

Before the ultimate aim can be realized it is necessary to adapt the oscillating-jet method to liquid-liquid systems. In the present work, we have developed the necessary mathematical framework and have studied the experimental techniques. The liquid-liquid jet is not yet at a stage where it can be used to determine mass-transfer behavior; however, a promising start has been made toward this goal.

The oscillating-jet phenomenon was reported independently by Bidone[7] in 1854 and Magnus[24] in 1855, but neither of them identified it with the surface tension of the liquids used.

In 1879 Lord Rayleigh[28] gave the first mathematical treatment in which the oscillations were correctly attributed to the surface-tension forces. When interpreted by the mathematical treatment he had developed, the measurements showed that the surface-tension values of

soap solutions were very near that of pure water for surface ages less than 0.001 sec (measured from the time the jet leaves the orifice).

Bohr[9] and Pedersen[27] in 1908 improved the experimental procedure. Both men also developed the mathematics further in order to be able to interpret their experiments more accurately. Bohr gave a fairly complete hydrodynamical treatment of the problem, which was more realistic than Pedersen's treatment. Bohr related the surface tension to the wavelength of the oscillations, the linear velocity, the maximum and minimum diameters of the stream, and the density and viscosity of the liquid. His main objective was a very accurate value for the surface tension of water with a freshly formed surface. He did not investigate any "dynamic" systems, in which the surface tension changes with time.

In 1920 Stocker[31] developed a very accurate method for measuring the wavelength of the oscillations, which involves passing a parallel beam of light through the stream perpendicular to its axis. The standing waves act as cylindrical converging lenses, which focus the light into a series of parallel lines on a photographic plate. A more complete discussion of this method is given in the experimental part of this dissertation.

In 1937 Bond and Puls[10] used the oscillating jet to check results obtained with their flowing-sheet method for the dynamic surface tension of some soap solutions. Their method consists of shooting two circular jets at each other, then measuring the diameter of the liquid disk formed from the collision. The age of the surface is calculated from the time required for the liquid to reach the perimeter of the liquid disk. They used the oscillating jet to check only one of their experiments; the results from the two methods agreed reasonably well.

Between 1943 and 1945 Addison[1-6] did a great deal of work on adsorption in alcohol-water solutions by using the oscillating jet. Avoiding Bohr's mathematics, Addison developed his own empirical relations. As part of his study, he undertook to adapt the oscillating jet to immiscible liquid-liquid systems. In such systems Bohr's mathematical treatment no longer applied, but Addison was able to

interpret his results by the same empirical method as for liquid-gas systems. From 1950 to 1953 Sutherland[32, 33] studied several systems with the oscillating jet, with use of Bohr's equations. On systems studied by both Sutherland and Addison, their results were noticeably different.

During this same period (1950 to 1953) Burcik[11-13] used the oscillating jet in a fundamental study of foams and emulsions. He determined that one of the important parameters in the stability of foams was the rate at which the surface tension changed. He studied this rate of change with the oscillating jet, but used Addison's empirical approach rather than Bohr's equation.

In recent work on liquid jets in air, Defay and Hommelen[16-18] have investigated the question of whether adsorption at the liquid-gas interface is controlled by diffusion or by some energy barrier that must be crossed to enter the interface. They studied two of the same systems studied by Sutherland and Addison. Their results agreed with Sutherland's, which throws some doubt on Addison's experiments or his empirical relations. Hansen and his co-workers,[21-23] interested in the same problem as Defay and Hommelen, have discussed the defects in Bohr's mathematical treatment (for the jet behavior very close to the nozzle) and have introduced semiempirical corrections to it. Thomas and Porter[36] have recently used a jet to study the effects of surface-active agents on hard water.

At this point it is appropriate to discuss the theory behind the oscillations of the jet. The reason it is possible to use this jet to measure interfacial tension is that the oscillations are a direct result of the interfacial tension. Thermodynamically speaking, the interfacial tension is the free energy per unit area. As the stream issues from the elliptical orifice in the form of an elliptical cylinder, the interfacial free energy is not at a minimum and hence the system is not in equilibrium. Therefore the stream tends toward the equilibrium configuration, which is a circular cylinder; however, the stream overshoots this equilibrium form, and then oscillates about it. This oscillation—when viewed from a point perpendicular to the axis of the

stream—gives the standing wave from which the experimental measurements are taken.

It is apparent that very little use of the oscillating jet has been made in liquid-liquid systems. It is very difficult to prevent the jet's breaking up within a path length too short for measurements to be made. Breakup occurs more easily due to the outside liquid's having higher viscosity and density than a gas. A second problem is the unavailability of suitable mathematical expressions, either empirical or theoretical, that would relate the wavelength of the oscillation to the interfacial tension.

II. STATEMENT OF THE PROBLEM

In this dissertation we deal with the problem of determining the interfacial tension between two immiscible liquids by using the oscillating-jet technique. Our ultimate objective, not yet reached, is one of using the oscillating jet to determine dynamic interfacial concentration during liquid-liquid mass transfer. The measurable parameter in this method is the wavelength produced by the oscillation.

The calculational problem is one of finding a suitable relation, either analytical or empirical, between wavelength and interfacial tension. The experimental problem is one of obtaining (a) suitable nozzles, (b) operating conditions that produce a maximum number of nodes in the jet and also a maximum total jet length, and (c) an optical assembly to provide high accuracy in measuring the wavelength and the minimum and maximum diameters of the jet. Because of the higher density, viscosity, and refractive index of the exterior fluid in a liquid-liquid system, both producing the jet and measuring it appear to be considerably more difficult than working with a liquid jet in air or other gas.

Thus the present study has been directed entirely toward the determination of equilibrium values of the interfacial tension.

III. MATHEMATICAL STUDY

A. Introduction

Bohr[9] has developed a mathematical treatment for calculating the surface tension of a single liquid, using the oscillating-jet technique. The objective of this section is to extend his mathematics to liquid-liquid systems. A rigorous attack on this problem, to solve exactly the Navier-Stokes equations describing it, is not possible. Hence, we must simplify the equations, but not to such an extent that their solution will no longer be physically valid. In order to meet this criterion, we have split the problem into two parts.

First, we have solved the Navier-Stokes equations with the same linearizing assumptions used by Bohr. We have assumed that the axial velocity is a constant plus a small perturbation, and that the radial and tangential velocities are only small perturbations. We do this for both phases since we must obtain a solution in each phase, and join them at the interface by using the boundary conditions. The perturbation velocities are caused by the oscillations of the jet. The solution thus obtained gives a relation between the wavelength and the interfacial tension; but it does not take into account the radial profile of the axial velocity, or the spreading of the jet. These important parameters are corrected for by the rest of the mathematical treatment.

The second part of the problem consists of a solution for the velocity profile in a circular liquid jet issuing into a second immiscible liquid. Two different methods have been used to solve the velocity problem. The first is an extension of Schlicting's solution[29] to the boundary-layer equations for a jet of liquid issuing into a large volume of the same liquid. The extension involves solving the boundary-layer equations for an inside liquid, and for an outside immiscible liquid of different physical properties, and then matching the solutions at the interface of the jet.

This treatment has some questionable characteristics. A solution can be obtained only for a jet issuing from an infinitely small orifice, and it is impossible to make the stress continuous at the

interface. In this treatment the jet is predicted to expand continuously after leaving the orifice; whereas, experimentally, the cross-sectional area of the jet is found first to contract and then to expand. Because of these departures from the physical situation, the solution obtained from the boundary-layer approximation with use of Schlicting's approach does not seem adequate.

A more realistic solution is suggested by the work of Okabe,[26] who used a method similar to that of von Karman and Polhausen[30] for obtaining an approximate solution to the boundary-layer equations. His solution, again for a liquid jet issuing into the same liquid, has the advantage of giving reasonable results at the orifice. In this method, a function assumed for the velocity profile contains several arbitrary parameters that are solved for by satisfying a set of physical conditions. This method should not be confused with the fitting of a function to experimental data, because the final velocity profile is determined without recourse to an experiment.

In our case we must fit nine conditions, outlined in Sec. C following. The function we have chosen is much simpler than Okabe's, but it satisfies all the necessary conditions and gives a velocity profile that appears realistic.

The next problem that confronts us is how to join the two mathematical results, so as to get one solution that best fits the physical situation. As there is no rigorous mathematical way of doing this, we resort to physical reasoning. In the oscillating-jet derivation, the same (constant) velocity is assumed for both the inside and outside phases. This is incorrect in two ways: neither the outside nor the inside velocity is constant, and the two velocities are equal only at the interface. To correct partly for this deficiency in the relation between wavelength and interfacial tension, we have replaced the velocity, in the terms pertaining to the inside liquid, by the average velocity of the jet calculated from the cylindrical-jet velocity profile. Also, the outside velocity has been replaced by the interfacial velocity calculated from the cylindrical velocity profile. It might seem that the inside velocity should be replaced by the interfacial velocity also, but—as

shown by trial numerical calculations—this does not take into account the total momentum of the jet.

One other correction allows for the fact that the amplitude of oscillation of the jet is not infinitesimally small, as has had to be assumed in order to solve the linearized differential equations. Bohr[9] developed this finite-amplitude correction with use of potential theory, and we have assumed that is also applicable to liquid-liquid systems. The correction is as follows:

$$\sigma = \sigma_{theor}\left(1 + \frac{37}{24}\,(r_i/r_x^{\,2})\right), \tag{1}$$

where

$$r_x = r_{max} + r_{min},$$

$$r_i = r_{max} - r_{min}.$$

B. Liquid-Liquid Oscillating Jet

The theory presented here is an extension of Bohr's fluid-dynamic analysis of the oscillating jet, to systems where the exterior fluid has appreciable viscosity and density. In this approach we have used reasonably simple mathematics, but have still tried to maintain a close correspondence to the actual physical situation.

The assumptions used will be explained at the point where they are first introduced, and then will be summarized at the end of this section. The method of attack will be to solve the equations of fluid motion (the Navier-Stokes equations), after linearization, in both liquid phases, and then to join the solutions at the interface with the appropriate boundary conditions.

The equations of viscous fluid motion for incompressible flow, in vector form, are

$$\rho \frac{D\vec{w}}{Dt} + \text{grad } P = \mu \nabla^2 \vec{w} ,$$

$$\text{div } \vec{w} = 0 . \tag{2}$$

These equations must be linearized before they can be solved. This will be done in rectangular coordinates, and they will then be transformed to cylindrical polar coordinates.

The rectangular coordinates are x, y, and z, and the respective velocities are g, h, and w. We assume that $w = c + \omega$, where c is constant; and that second-order terms in g, h, and ω will be small enough to drop. We also assume that the waveform—and therefore the velocities—will be sinusoidal; i. e., of the form

$$f(x, y) e^{ibz} .$$

Thus b is the wave number $2\pi/\lambda$, with λ the wavelength. The Navier-Stokes equations, in linearized form, are then

$$\left(\nabla^2 - \frac{ibc\rho}{\mu}\right) g = \frac{1}{\mu} \frac{\partial P}{\partial x} , \tag{3}$$

$$\left(\nabla^2 - \frac{ibc\rho}{\mu}\right) h = \frac{1}{\mu} \frac{\partial P}{\partial y} , \tag{4}$$

$$\left(\nabla^2 - \frac{ibc\rho}{\mu}\right) \omega = \frac{1}{\mu} \frac{\partial P}{\partial z} . \tag{5}$$

It is necessary to solve for the pressure P before the velocities can be obtained; P is obtained from the above linearized equations; as is more evident from their vector form, Eq. (2). We take the divergence of Eq. (1), and interchange operations where permissible:

$$\rho \frac{D}{Dt} (\text{div } \vec{w}) + \text{div grad } P = \mu \nabla^2 (\text{div } \vec{w}) .$$

Since $\operatorname{div} \vec{w} = 0$, we obtain

$$\operatorname{div} \operatorname{grad} P = \nabla^2 P = 0 \,. \tag{6}$$

Solution of the linearized momentum relations, Eqs. (3) through (5), is much easier if they are made homogeneous. To do this we use the following transformations:

$$g = g_1 + \frac{i}{cb\rho} \frac{\partial P}{\partial x},$$

$$h = h_1 + \frac{i}{cb\rho} \frac{\partial P}{\partial y}, \tag{7}$$

$$\omega = \omega_1 + \frac{i}{cb\rho} \frac{\partial P}{\partial z}.$$

The momentum equations thus become

$$\left(\nabla^2 - \frac{ibc\rho}{\mu}\right) g_1 = 0, \tag{8}$$

$$\left(\nabla^2 - \frac{ibc\rho}{\mu}\right) h_1 = 0, \tag{9}$$

$$\left(\nabla^2 - \frac{ibc\rho}{\mu}\right) \omega_1 = 0, \tag{10}$$

and the equation of continuity, Eq. (2), remains:

$$\frac{\partial g_1}{\partial x} + \frac{\partial h_1}{\partial y} + \frac{\partial \omega_1}{\partial z} = 0 \,. \tag{11}$$

Now we transform to cylindrical polar coordinates r, θ, and z by the following transformations:

$$x = r \cos \theta \,, \qquad y = r \sin \theta \,, \tag{12}$$

$$g = v \cos\theta - u \sin\theta , \qquad g_1 = v_1 \cos\theta - u_1 \sin\theta ,$$

$$h = v \sin\theta + u \cos\theta , \qquad h_1 = v_1 \sin\theta + u_1 \cos\theta , \tag{13}$$

$$\frac{\partial}{\partial x} = \cos\theta \frac{\partial}{\partial r} - \frac{\sin\theta}{r} \frac{\partial}{\partial \theta} ,$$

$$\frac{\partial}{\partial y} = \sin\theta \frac{\partial}{\partial r} + \frac{\cos\theta}{r} \frac{\partial}{\partial \theta} . \tag{14}$$

A further transformation makes the momentum equations in cylindrical coordinates homogeneous in the same manner as for rectangular coordinates:

$$v = \frac{i}{cb\rho} \frac{\partial P}{\partial r} + v_1 ,$$

$$u = \frac{i}{cb\rho} \frac{1}{r} \frac{\partial P}{\partial \theta} + u_1 . \tag{15}$$

The equations of motion (linearized and homogeneous), in cylindrical polar coordinates, as obtained by Bohr, are

$$\left(\nabla^2 - \frac{ibc\rho}{\mu}\right) v_1 - \frac{v_1}{r^2} - \frac{2}{r^2} \frac{\partial u_1}{\partial \theta} = 0 , \tag{16}$$

$$\left(\nabla^2 - \frac{ibc\rho}{\mu}\right) u_1 - \frac{u_1}{r^2} + \frac{2}{r^2} \frac{\partial v_1}{\partial \theta} = 0 , \tag{17}$$

$$\left(\nabla^2 - \frac{ibc\rho}{\mu}\right) \omega_1 = 0 , \tag{18}$$

$$\frac{\partial v_1}{\partial r} + \frac{v_1}{r} + \frac{1}{r} \frac{\partial u_1}{\partial \theta} + \frac{\partial \omega_1}{\partial z} = 0 . \tag{19}$$

In the following we assume (with Bohr) that u_1, v_1, ω_1, and P are all of the form

$$\sum_{n=0}^{\infty} f(r)e^{in\theta+ibz} .$$

This is actually a Fourier (trigonometric) expansion of the velocities and pressure. However, we need only the term for $n = 2$ because this corresponds to the type of perturbation we have imposed on the stream; i.e., we have forced the liquid through an elliptical opening. In other words, we use the term that corresponds to an n-fold (in this case, 2-fold) axis of symmetry for the jet. The periodicity in the z direction matches the assumption already made.

The order of solution will be to solve first for P and then ω_1. Next we solve the radial-momentum and continuity equations for v_1; and finally we integrate the continuity equation to obtain the function for u_1.

With P in the above form, the pressure equation is

$$\nabla^2 P = \frac{d^2P}{dr^2} + \frac{1}{r}\frac{dP}{dr} - P\left(\frac{n^2}{r^2} + b^2\right) = 0 . \tag{20}$$

This is a form of Bessel's equation, which has the solution

$$P = A_1 I_n(br) + A_2 K_n(br) . \tag{21}$$

The complete solution is

$$P = [A_1 I_n(br) + A_2 K_n(br)]\, e^{in\theta+ibz} . \tag{22}$$

The momentum equation for the z direction, Eq. (18), can be written in the same general form as the pressure equation:

$$\frac{d^2\omega_1}{dr^2} + \frac{1}{r}\frac{d\omega_1}{dr} - \omega_1\left(\frac{n^2}{r^2} + d^2\right) = 0 , \tag{23}$$

with d (an indirect measure of the wavelength) defined as:

$$d^2 = b^2 + \frac{ibc\rho}{\mu} . \tag{24}$$

The solution, with the same form as for P, is

$$\omega_1 = [B_1 I_n(dr) + B_2 K_n(dr)] e^{in\theta+ibz} . \tag{25}$$

From the continuity and the radial-momentum relations, Eqs. (19) and (16), we get

$$r\left(\nabla^2 - \frac{ibc\rho}{\mu}\right)v_1 + 2\frac{\partial v_1}{\partial r} + \frac{v_1}{r} = -2\frac{\partial \omega_1}{\partial z} , \tag{26}$$

which can be rewritten as

$$\left(\nabla^2 - \frac{ibc\rho}{\mu}\right)(rv_1) = -2ib\,[B_1 I_n(dr) + B_2 K_n(dr)]\, e^{in\theta+ibz} . \tag{27}$$

The above equation contains a nonhomogeneous part, which requires introduction of the following operator identity:

$$\left(\nabla^2 - \frac{ibc\rho}{\mu}\right)\left(r\frac{\partial}{\partial r}\right) = \left(r\frac{\partial}{\partial r}\right)\left(\nabla^2 - \frac{ibc\rho}{\mu}\right) + 2\frac{\partial^2}{\partial r^2} + \frac{2}{r}\frac{\partial}{\partial r} + \frac{2}{r^2}\frac{\partial^2}{\partial \theta^2}$$

$$= \left(r\frac{\partial}{\partial r} + 2\right)\left(\nabla^2 - \frac{ibc\rho}{\mu}\right) - 2\left(\frac{\partial^2}{\partial z^2} - \frac{ibc\rho}{\mu}\right). \tag{28}$$

If we perform the indicated operations upon

$$[B_1 I_n(dr) + B_2 K_n(dr)]\, e^{in\theta+ibz} ,$$

we get

$$\left(\nabla^2 - \frac{ibc\rho}{\mu}\right)\left\{r\,\frac{\partial}{\partial r}\,[B_1 I_n(dr) + B_2 K_n(dr)]\,e^{in\theta+ibz}\right\}$$

$$= 2\left(b^2 + \frac{ibc\rho}{\mu}\right)\left(B_1 I_n(dr) + B_2 K_n(dr)\right) e^{in\theta+ibz} \quad . \tag{29}$$

Except for a constant multiplier, the right-hand side of Eq. (29) is the nonhomogeneous part of the solution of Eq. (27), which we designate as $(v_1)_{nh}$

$$(v_1)_{nh} = -\frac{ib}{d^2}\,[B_1 I_n(dr) + B_2 K_n(dr)]\,e^{in\theta+ibz} \quad . \tag{30}$$

The homogeneous part of the solution of Eq. (27) is

$$(v_1)_h = [C_1 I_n(dr) + C_2 K_n(dr)]\,e^{in\theta+ibz} \quad . \tag{31}$$

Combining these we obtain

$$v_1 = (v_1)_{nh} + (v_1)_h =$$

$$\left\{\frac{1}{r}\,[C_1 I_n(dr) + C_2 K_n(dr)] - \frac{ib}{d^2}\,[B_1 I_n(dr) + B_2 K_n(dr)]\right\} e^{in\theta+ibz} \quad . \tag{32}$$

Having obtained this solution for v_1, we can use it in solving for u_1. The continuity equation, (19), integrates to

$$-u_1 = r\int\left(\frac{\partial\,\omega_1}{\partial z} + \frac{v_1}{r} + \frac{\partial\,v_1}{\partial r}\right)d\theta \quad . \tag{33}$$

Substitution from Eqs. (25) and (32), and integration over θ, give

$$- u_1 = r \Big\{ ib\,[B_1 I_n(dr) + B_2 K_n(dr)] + \frac{1}{r^2}\,[C_1 I_n(dr) + C_2 K_n(dr)]$$

$$- \frac{ib}{rd^2}\,[B_1 I_n'(dr) + B_2 K_n'(dr)] + \frac{1}{r}\,[C_1 I_n'(dr) + C_2 K_n'(dr)]$$

$$- \frac{1}{r^2}\,[C_1 I_n(dr) + C_2 K_n(dr)] - \frac{ib}{d^2}\,[B_1 I_n''(dr) + B_2 K_n''(dr)]\Big\} \int e^{in\theta + ibz} d\theta. \tag{34}$$

From the properties of the Bessel functions, we have

$$\left.\begin{aligned} I_n''(a) + \frac{1}{r}\, I_n'(a) - I_n(a)\left(\frac{n^2}{r^2} + d^2\right) &= 0 \\ K_n''(a) + \frac{1}{r}\, K_n'(a) - K_n(a)\left(\frac{n^2}{r^2} + d^2\right) &= 0\,. \end{aligned}\right\} \tag{35}$$

These relations simplify the preceding integral to the solution form

$$u_1 = \Big\{ \frac{i}{n}\,[C_1 I_n'(dr) + C_2 K_n'(dr)] + \frac{nb}{dr^2}\,[B_1 I_n(dr)$$

$$+ B_2 K_n(dr)]\Big\}\, e^{in\theta + ibz}\,. \tag{36}$$

In the liquid-liquid jet we need a solution for both the inside and the outside fluid. It is possible to adapt the above solutions for the velocities to this situation, by noting that the velocity must be finite at $r \to 0$ and $r \to \infty$. Therefore, for the inside fluid, the coefficients of the modified Bessel functions of the second kind (K_n, K_n') must be zero; and, for the outside, the coefficients of the modified Bessel functions of the first kind (I_n, I_n') must be zero.

For the inside fluid, we get

$$w_i = c + \omega_i = c + [B_1 I_2(d_i r) - \frac{A_1}{c\rho_i}\, I_2(br)]\, e^{in\theta + ibz}\,, \tag{37}$$

$$v_i = \left[\frac{C_1}{r} I_2(d_i r) - \frac{ib}{d_i^2} B_1 I_2'(d_i r) + \frac{i}{cb\rho_i} A_1 I_2'(br)\right] e^{in\theta+ibz} , \quad (38)$$

$$u_i = \left[\frac{iC_1}{2} I_2'(d_i r) + \frac{2bB_1}{rd_i^2} I_2(d_i r) - \frac{2}{cb\rho_i} \frac{1}{r} A_1 I_2(br)\right] e^{in\theta+ibz} . \quad (39)$$

For the exterior fluid, also, we have

$$w_e = c + \omega_e = c + \left[B_2 K_2(d_e r) - \frac{1}{c\rho_e} A_2 K_2(br)\right] e^{in\theta+ibz} , \quad (40)$$

$$v_e = \left[\frac{C_2}{r} K_2(d_e r) - \frac{ib}{d_e^2} B_2 K_2'(d_e r) + \frac{i}{bc\rho_e} A_2 K_2'(br)\right] e^{in\theta+ibz} , \quad (41)$$

$$u_e = \left[\frac{iC_2}{2} K_2'(d_e r) + \frac{2b}{rd_e^2} B_2 K_2(d_e r) - \frac{2}{cb\rho_e} \frac{1}{r} A_2 K_2(br)\right] e^{in\theta+ibz} . \quad (42)$$

1. Boundary Conditions

In obtaining the preceding velocity equations, we have used six of the available boundary conditions. However, the velocity equations contain six additional arbitrary constants which must be solved for with six additional boundary conditions. Stated in words, these boundary conditions are: The three velocities must be continuous at the interface; and the normal, tangential, and axial stresses must be continuous at the interface. These conditions may be written mathematically as follows:

1. $r = a, \quad w_i = w_e ,$
2. $r = a, \quad v_i = v_e ,$
3. $r = a, \quad u_i = u_e ,$
4. $r = a, \quad -P_e + 2\mu_e \frac{\partial v_e}{\partial r} = -P_i + 2\mu_i \frac{\partial v_i}{\partial r} + \sigma \left(\frac{1}{R_1} + \frac{1}{R_2}\right),$

5. $r = a,$ $$\mu_e\left(\frac{\partial w_e}{\partial r} + \frac{\partial v_e}{\partial z}\right) = \mu_i\left(\frac{\partial w_i}{\partial r} + \frac{\partial v_i}{\partial z}\right),$$

6. $r = a,$ $$\mu_e\left(\frac{\partial u_e}{\partial r} - \frac{u_e}{r} + \frac{1}{r}\frac{\partial v_e}{\partial \theta}\right) = \mu_i\left(\frac{\partial u_i}{\partial r} - \frac{u_i}{r} + \frac{1}{r}\frac{\partial v_e}{\partial \theta}\right).$$

In condition 4, σ is the interfacial tension, and R_1 and R_2 are the principle radii of curvature of the surface. We must find relations for R_1 and R_2 in terms of our velocities and coordinate system.

2. Radii of Curvature of the Interface

We assume an equation for the surface of the form

$$r - a = \zeta = Q\, e^{in\theta + ibz}, \tag{43}$$

with $n = 2$, as explained previously. The general surface condition, which states that the jet is bounded by its surface, gives

$$\frac{D}{Dt}(r - a - \zeta) = \left(v_i \frac{\partial}{\partial r} + \frac{u_i}{r}\frac{\partial}{\partial \theta} + w_i \frac{\partial}{\partial z}\right)(r - a - \zeta) = 0 . \tag{44}$$

If we neglect second-order terms in velocity, as has been done previously, we have

$$v - c\frac{\partial \zeta}{\partial z} = 0 . \tag{45}$$

Then

$$\zeta = -\frac{i}{cb} v_i . \tag{46}$$

It is now possible to determine R_1 and R_2 in terms of v_i, from Eq. (46):

$$\frac{1}{R_1} + \frac{1}{R_2} = \left(\frac{1}{a} - \frac{\zeta}{a^2}\right) + \left(-\frac{1}{a^2}\frac{\partial^2 \zeta}{\partial \theta^2} - \frac{\partial^2 \zeta}{\partial z^2}\right) \tag{47}$$

$$= \frac{1}{a} - v_i \left(\frac{i}{a^2 cb}\right)(3 + b^2 a^2) . \tag{48}$$

This expression will be used in the normal-stress boundary condition.

3. The Expression for σ

If we now substitute the proper quantities, obtained from the velocity relations, into the boundary conditions, we obtain six equations in six unknowns. The unknowns are the six arbitrary constants A_1, A_2, B_1, B_2, C_1, and C_2. The six equations are:

$$B_1 I_2(d_i a) - B_2 K_2(d_e a) - \frac{A_1}{c\rho_i} I_2(ba) + \frac{A_2}{c\rho_e} K_2(ba) = 0 , \tag{49}$$

$$\frac{C_1}{a} I_2(d_i a) - \frac{C_2}{a} K_2(d_e a) - \frac{ibB_1}{d_i^2} I_2'(d_i a) + \frac{ibB_2}{d_e^2} K_2'(d_e a)$$

$$+ \frac{iA_1}{cb\rho_i a} I_2'(ba) - \frac{iA_2}{cb\rho_e a} K_2'(ba) = 0 , \tag{50}$$

$$\frac{iC_1}{2} I_2'(d_i a) - \frac{iC_2}{2} K_2'(d_e a) + \frac{2bB_1}{ad_i^2} I_2(d_i a) - \frac{2bB_2}{ad_e^2} K_2(d_e a)$$

$$- \frac{2}{c\rho_i ba} A_1 I_2(ba) + \frac{2}{c\rho_e ba} A_2 K_2(ba) = 0 , \tag{51}$$

$$A_1\left[2\mu_i \frac{i}{cb\rho_i} I_2''(ba) - I_2(ba) - \frac{\sigma Li}{cb\rho_i} I_2'(ba)\right] + A_2\left[K_2(ba) - \frac{2\mu_e i}{cb\rho_e} K_2''(ba)\right]$$

$$+ B_1\left[\frac{\sigma Lib}{d_i^2} I_2'(d_i a) - 2\mu_i \frac{ib}{d_i^2} I_2'(d_i a)\right] + B_2\left[2\mu_e \frac{ib}{d_e^2} K_2'(d_e a)\right]$$

$$+C_2\left(\frac{2\mu_e}{a}\right)\left[\frac{1}{a}K_2(d_e a) - K_2'(d_e a)\right] + \frac{C_1}{a}\left\{2\mu_i\left[I_2'(d_i a) - \frac{I_2}{a}(d_i a)\right] - \sigma L I_2(d_i a)\right\} = 0, \tag{52}$$

$$- A_1\left[\frac{2\mu_i}{c\rho_i} I_2'(ba)\right] + A_2\left[\frac{2\mu_e}{c\rho_e} K_2'(ba)\right] + B_1\mu_i\left[\left(1 + \frac{b^2}{d_i^2}\right) I_2'(d_i a)\right]$$

$$- B_2\mu_e\left[\left(1 + \frac{b^2}{d_e^2}\right) K_2'(d_e a)\right] + \left[\mu_i C_1 \frac{ib}{a} I_2(d_i a)\right] - \left[\mu_e C_2 \frac{ib}{a} K_2(d_e a)\right] = 0, \tag{53}$$

$$A_1\left(\frac{4\mu_i}{cb\rho_i a}\right)\left[\frac{I_2(ba)}{a} - I_2''(ba)\right] + B_1\left(\frac{4\mu_i b}{ad_i^2}\right)\left[I_2'(d_i a) - \frac{I_2(d_i a)}{a}\right]$$

$$+ C_1 (i\mu_i)\left[\frac{I_2'(d_i a)}{2} - \frac{I_2'(d_i a)}{2a} + \frac{2I_2(d_i a)}{a^2}\right]$$

$$- A_2\left(\frac{4\mu_e}{cb\rho_e a}\right)\left[\frac{K_2(ba)}{a} - K_2'(ba)\right] - B_1\left(\frac{4\mu_e b}{ad_e^2}\right)\left[K_2'(d_e a) - \frac{K_2(d_e a)}{a}\right]$$

$$- C_2 (i\mu_e)\left[\frac{K_2'(d_e a)}{2} - \frac{K_2'(d_e a)}{2a} + \frac{2K_2(d_e a)}{a^2}\right] = 0, \tag{54}$$

$$L \equiv \frac{i(3 + a^2b^2)}{a^2cb}.$$

The equations are cumbersome; as they would be extremely difficult to solve by hand, they have been evaluated instead on an IBM 7090 computer. The equations are homogeneous and therefore have the property that the determinant of the coefficients of the arbitrary constants must be zero for a nontrivial solution to exist. We have no real interest in the arbitrary constants themselves; but are interested only in a relation between the interfacial tension and the wavelength of oscillation. The above-mentioned determinant furnishes this relation.

A dummy determinant is used here to describe the method used to obtain the interfacial tension. The quantities x_{ij}, represent terms containing the densities and viscosities of the two fluids plus the dimensions of the jet.

$$\begin{vmatrix} x_{11} & x_{12} & x_{13} & x_{14} & x_{15} & x_{16} \\ x_{21} & x_{22} & x_{23} & x_{24} & x_{25} & x_{26} \\ x_{31} & x_{32} & x_{33} & x_{34} & x_{35} & x_{36} \\ x_{41} + \sigma K_1 & x_{42} & x_{43} + \sigma K_2 & x_{44} & x_{45} + \sigma K_3 & x_{46} \\ x_{51} & x_{52} & x_{53} & x_{54} & x_{55} & x_{56} \\ x_{61} & x_{62} & x_{63} & x_{64} & x_{65} & x_{66} \end{vmatrix} = 0 . \tag{55}$$

This determinant may be separated into two determinants in the following manner:

$$\begin{bmatrix} x_{ij} \end{bmatrix}_{\substack{i = 1 \cdots 6 \\ j = 1 \cdots 6}} + \sigma \begin{vmatrix} x_{11} & x_{12} & x_{13} & x_{14} & x_{15} & x_{16} \\ x_{21} & x_{22} & x_{23} & x_{24} & x_{25} & x_{26} \\ x_{31} & x_{32} & x_{33} & x_{34} & x_{35} & x_{36} \\ K_1 & 0 & K_2 & 0 & K_3 & 0 \\ x_{51} & x_{52} & x_{53} & x_{54} & x_{55} & x_{56} \\ x_{61} & x_{62} & x_{63} & x_{64} & x_{65} & x_{66} \end{vmatrix} = 0 . \tag{56}$$

If we designate the first determinant D, and the second Δ, then

$$\sigma = - \frac{D}{\Delta} . \tag{57}$$

This equation was solved numerically on the computer. The method used was a standard Gauss-reduction method. The actual program used, which is written in Fortran language, is included in Appendix B.

Thus the solution is obtained in the implicit functional form,

$$\text{fn.}\,(\sigma,\ c,\ a,\ b,\ \rho_i,\ \mu_i,\ \rho_e,\ \mu_e) = 0\,,$$

with $b = 2\pi/\lambda$. When these terms are assembled into dimensionless groups, and solved explicitly for σ, we have

$$\frac{\sigma}{\rho_i c^2 a_0} = \text{fn.}\left(\frac{c a_0 \rho_i}{\mu_i},\ \frac{2\pi a_0}{\lambda},\ \frac{\rho_e}{\rho_i},\ \frac{\mu_e}{\mu_i}\right).$$

This can be interpreted to read that the reciprocal of the Weber number is a function of the inside Reynolds number, the dimensionless wave number, the density ratio, and the viscosity ratio. To show the nature of the exact relations given by Eqs. (55) through (57), we have evaluated the reciprocal Weber number in terms of the other dimensionless groups, by using three separate numerical values each for Reynolds number and wave number, and five pairs of values for density ratio and viscosity ratio. The results are shown in Figs. 1 through 5. These figures can be used for interpolation, with less accuracy but also much less effort than is involved in solving the six-by-six determinant. The amplitude correction, Eq. (1), is not included in the dimensionless plots, and must be used to correct the value taken from the plots.

For very rough approximations, i.e., to obtain values within 50% or so of the correct calculated values, we have developed the following equation:

$$\frac{\sigma}{\rho_i c^2 a_0} = 0.114\left(\frac{2\pi a_0}{\lambda}\right)^{1.67}\left(\frac{\rho_e}{\rho_i} + 1.18\right). \tag{58}$$

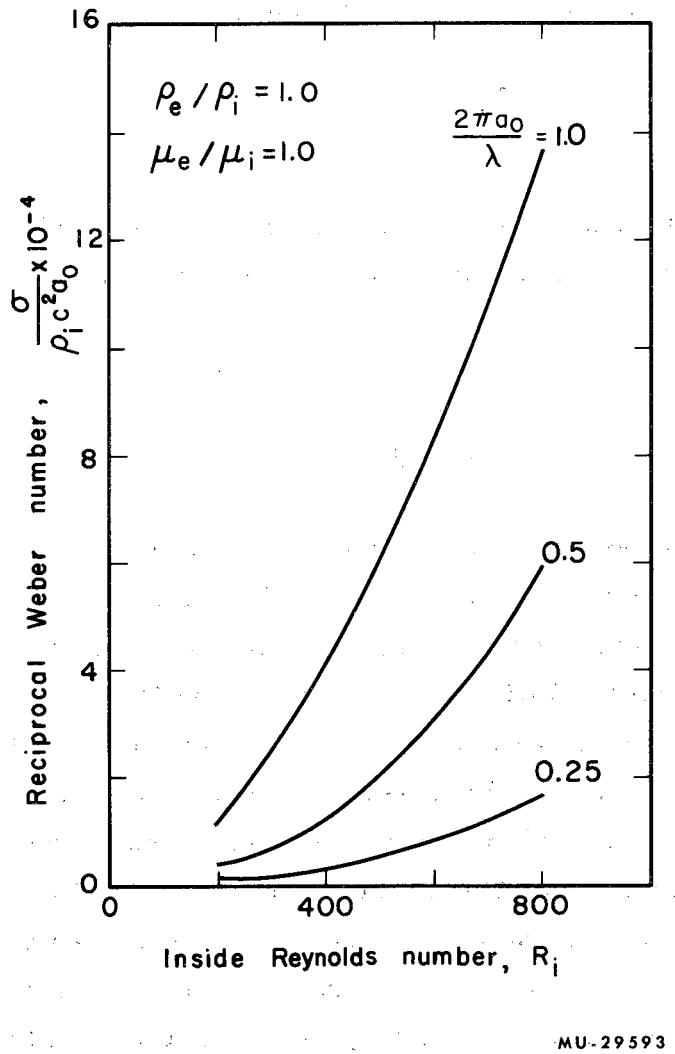

Fig. 1. Relation between dimensionless parameters defining oscillating-jet behavior. Density ratio, 1.0; viscosity ratio, 1.0.

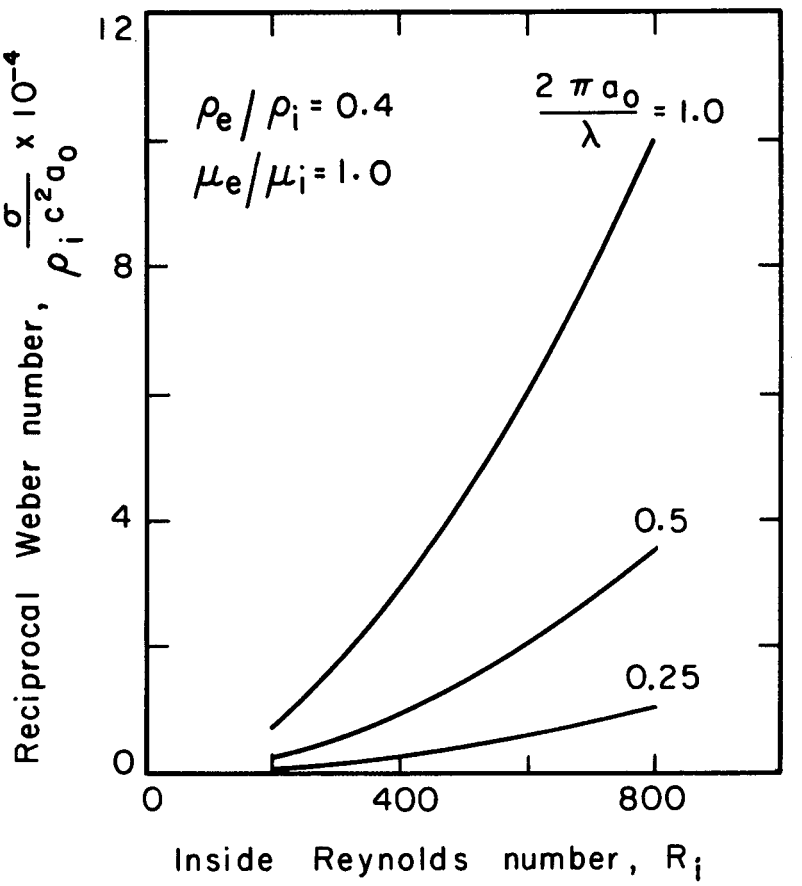

MU-29949

Fig. 2. Relation between dimensionless parameters defining oscillating-jet behavior. Density ratio, 0.4; viscosity ratio, 1.0.

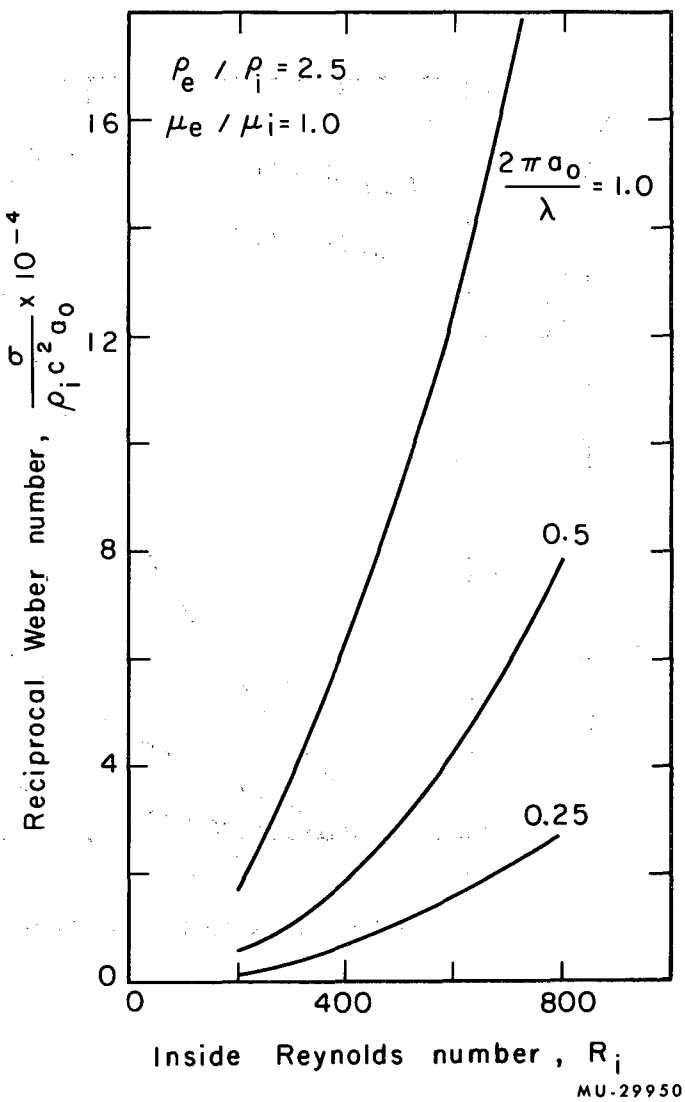

Fig. 3. Relation between dimensionless parameters defining oscillating-jet behavior. Density ratio, 2.5; viscosity ratio, 1.0.

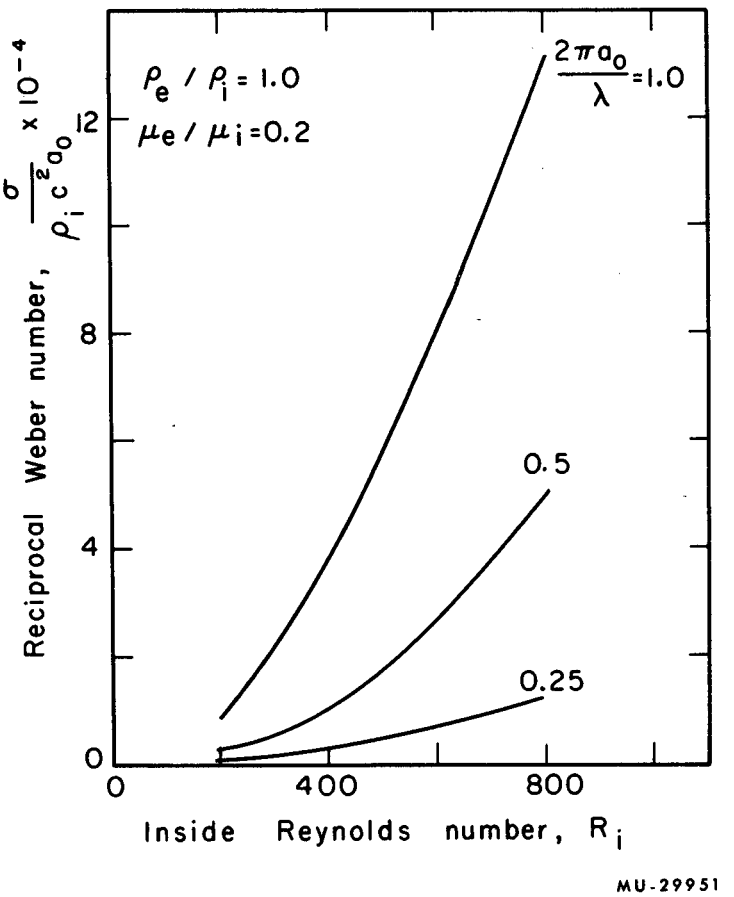

Fig. 4. Relation between dimensionless parameters defining oscillating-jet behavior. Density ratio, 1.0; viscosity ratio, 0.2.

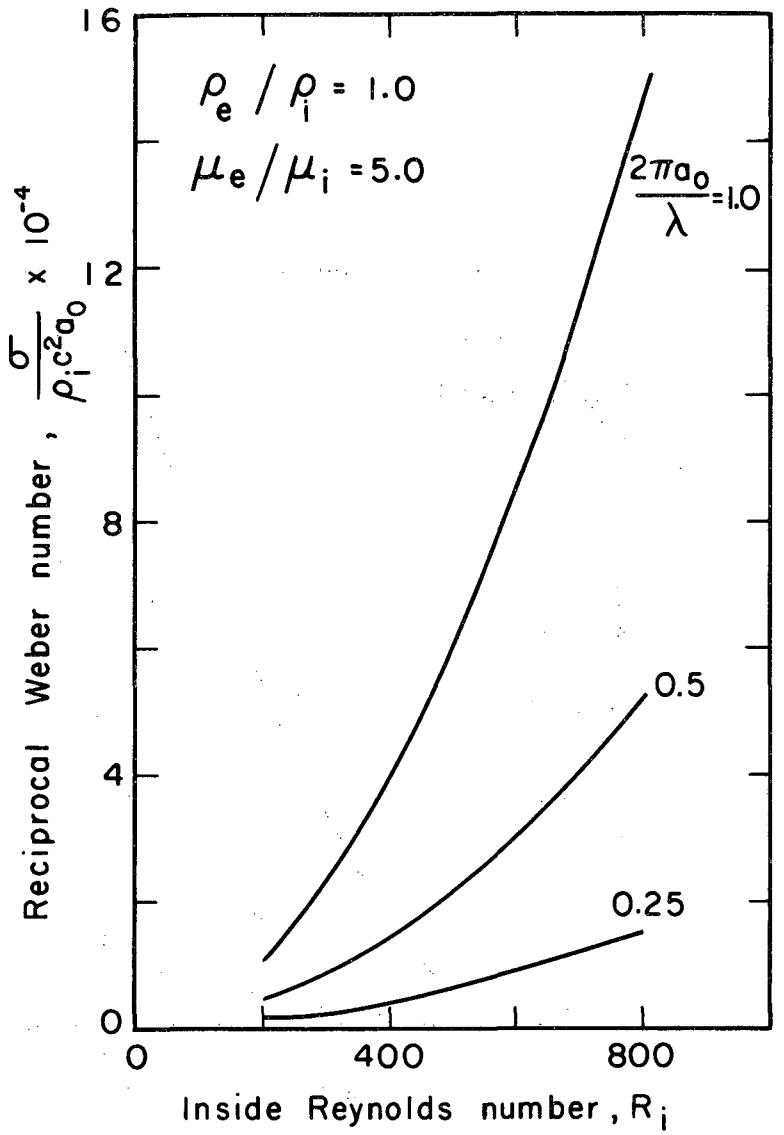

MU-29952

Fig. 5. Relation between dimensionless parameters defining oscillating-jet behavior. Density ratio, 1.0; viscosity ratio, 5.0.

This expression was obtained with use of a viscosity ratio of 1.0, and should be used only when a "general-neighborhood" value is desired.

4. Summary of Assumptions

The assumptions made in linearizing the Navier-Stokes equations were similar to those made by Stokes for solution of the creeping-flow problem. The difference is that we assumed the axial velocity had an added constant. Physically, this means that the axial velocity is assumed to be a plug-type profile on which we impose a small perturbation. This is not the type of profile actually encountered in the experiments. For this reason the next section develops a correction for the velocity variation of the profile.

The assumption made about the type of wave pattern encountered, i.e. sinusoidal, should be very good. Pictures of experimental jets have shown that the oscillation can be approximated very well by this assumption.

The final important assumption was made in solving the determinants to obtain the interfacial tension. The quantity b is actually of the form

$$b = b_0 + i\epsilon .$$

Here $b_0 = 2\pi/\lambda$ and ϵ is the damping factor on the oscillations. We have had to assume that $b = 2\pi/\lambda$, which would be true if ϵ is very small. This assumption must be made because our final answer is not explicit in b; i.e., at the conclusion of the calculation, we cannot separate b into its real and imaginary parts. In fact we must begin the calculation with a value of b in order to obtain the interfacial tension.

The assumption that ϵ is small compared with b_0 is physically inexact, but in most cases probably not a large source of numerical error. In the case solved by Bohr, it was possible to find ϵ and it was indeed much smaller than b_0. Since we could not separate b

into its real and imaginary parts, the interfacial tension calculated had a small imaginary part which we disregarded.

C. Velocity Profile of a Cylindrical Immiscible Liquid-Liquid Jet

The preceding section led to a mathematical relation between the wavelength and the interfacial tension for an oscillating jet. To obtain this relation, we assumed that the velocity in the axial direction had a constant profile, realizing that this is not a good assumption. In this section we derive an axial velocity profile (in two different ways), and use the result to correct the relation between interfacial tension and wavelength.

1. Schlicting - Type Solution

The Navier-Stokes equations for an incompressible fluid under boundary-layer type approximations, for the case of an axially symmetric jet, reduce to the following:

$$\bar{w}\,\frac{\partial \bar{w}}{\partial \bar{z}} + \bar{v}\,\frac{\partial \bar{w}}{\partial \bar{r}} = \nu\left(\frac{1}{\bar{r}}\,\frac{\partial \bar{w}}{\partial \bar{r}} + \frac{\partial^2 \bar{w}}{\partial \bar{r}^2}\right),$$

$$\frac{\partial \bar{w}}{\partial \bar{z}} + \frac{\bar{v}}{\bar{r}} + \frac{\partial \bar{v}}{\partial \bar{r}} = 0, \tag{59}$$

where $\nu = \mu/\rho$. It is possible to make these equations dimensionless by dividing the length terms by a_0, the radius of the orifice, and the velocities by w_0, the average velocity in the orifice. We thus obtain

$$r = \frac{\bar{r}}{a_0},\ z = \frac{\bar{z}}{a_0},\ w = \frac{\bar{w}}{w_0}, \qquad \text{and} \qquad v = \frac{\bar{v}}{a_0}.$$

The boundary-layer equations may now be written

$$w \frac{\partial w}{\partial z} + v \frac{\partial w}{\partial r} = \frac{\nu}{a_0 w_0} \left[\frac{1}{r} \frac{\partial w}{\partial r} + \frac{\partial^2 w}{\partial r^2} \right] , \tag{60}$$

$$\frac{\partial w}{\partial z} + \frac{v}{r} + \frac{\partial v}{\partial r} = 0 . \tag{61}$$

Schlicting[29] has solved this case, when both the jet liquid and the exterior liquid are the same or have the same densities and viscosities, by using the following transformations:

$$\phi = \frac{x}{R} h(\eta), \qquad \eta = \sqrt{R \frac{r}{x}} . \tag{62}$$

Here ϕ is the stream function, η is a "similarity" variable, and R is the Reynolds number $a_0 w_0 / \nu$. To obtain the preceding form of the boundary-layer equations, the pressure in the z direction is assumed constant; hence, the total momentum in the z direction is constant at all points downstream. The momentum balance may be written

$$2\pi \int_0^\infty \rho w^2 r dr = \text{constant} . \tag{63}$$

Use of this similarity-variable treatment makes the velocity infinite at the orifice, with the orifice being infinitesimally small in order that the mass flow rate and momentum remain finite. To make the solution physically usable, it must be truncated at a value of x greater than zero. As an arbitrary but probably optimum choice, truncation is made where the radius of the jet is a_0.

Since there are two regions physically, corresponding to the two different liquids, the equations must be solved in both regions and joined at the interface by appropriate boundary conditions. The velocities in terms of the stream function ϕ, for either phase, are

$$w = - \frac{1}{r} \frac{\partial \phi}{\partial r}, \qquad v = - \frac{1}{r} \frac{\partial \phi}{\partial z} . \tag{64}$$

The transformed equation is thus

$$\frac{d}{d\eta}\left(h'' - \frac{h'}{\eta} + \frac{hh'}{\eta}\right) = 0 . \tag{65}$$

This third-order nonlinear differential equation requires six boundary conditions to give a solution for both the interior and exterior phases. The following boundary conditions are used:

1. $r = 0: \quad \partial w_i/\partial r = 0 ,$

2. $r = 0: \quad v_i = 0 ,$

3. $r = a: \quad w_i = w_e ,$

4. $r = a: \quad v_i = v_e ,$

5. $r \to \infty: \quad w_e \to 0 ,$

6. Constant momentum, from Eq. (63):

$$\int_0^a w_i^2 r dr + \frac{\rho_2}{\rho_1} \int_a^\infty w_e^2 r dr = \text{constant}.$$

We first apply Eq. (65) to the interior phase:

$$\frac{d}{d\eta} h_i' - \frac{h_i'}{\eta} + \frac{h_i h_i'}{\eta} = 0 . \tag{66}$$

This may be integrated once to give

$$h_i'' - \frac{h_i'}{\eta} + \frac{h_i h_i'}{\eta} = C_1 . \tag{67}$$

From boundary conditions 1 and 2, both h and h' are zero at

$\eta = 0$. Expansion of the equation in a Taylor's series about $\eta = 0$ gives $C_1 = 0$. Equation (67) can be integrated again to give

$$\eta h_i' - 2h_i + \frac{h_i^2}{2} = C_2 . \tag{68}$$

The constant C_2 is also zero, since the velocity must remain finite for $\eta = 0$.

For the outside liquid, Eq. (65) can be integrated again to give:

$$h_e'' - \frac{h_e'}{\eta} + \frac{h_e h_e'}{\eta} = C_3 . \tag{69}$$

The constant C_3 must be zero because h_e'', h_e', and h_e all must remain finite as $\eta \to \infty$. Integrating a second time, we get

$$\eta h_e' - 2h_e + \frac{h_e^2}{2} = C_4 . \tag{70}$$

The derived differential equations are still nonlinear, but first-order, and are forms of the Riccati equation. They are reduced to linear equations by the transformation

$$h = \frac{2\eta}{y} \frac{dy}{d\eta} . \tag{71}$$

The inside equation becomes

$$y'' - \frac{y'}{\eta} = 0 . \tag{72}$$

This is solved by two quadratures, and then is transformed by Eq. (71) back to

$$h_i = \frac{4\eta^2}{\eta^2 + A} . \tag{73}$$

The outside-fluid equation transforms, by Eq. (71), to

$$y'' - \frac{y'}{\eta} - \frac{C_4}{2\eta^2 y} = 0 . \tag{74}$$

This corresponds to the Euler equation; integration, followed by back-transformation, yields

$$he = 2 \left[1 + \gamma \left(\frac{\eta^{\gamma} - B\eta^{-\gamma}}{\eta^{\gamma} + B\eta^{-\gamma}} \right) \right] , \tag{75}$$

where

$$\gamma = \sqrt{1 + (C_4/2)} .$$

In terms of the original variables, the velocities become, inside:

$$w_i = \frac{8\ Az^3}{(r^2 R_i + Az^2)^2} , \tag{76}$$

$$v_i = \frac{4\, r(Az^2 - r^2 R_i)}{(r^2 R_i + Az^2)^2} , \tag{77}$$

and outside:

$$w_e = \frac{2\, z}{R_e} \left(\frac{\gamma}{r} \right)^2 \left(1 - L_2{}^2 \right) , \tag{78}$$

$$v_e = \frac{2}{r R_e} \left[\gamma^2 (1 - L_2{}^2) - (1 + \gamma L_2) \right] , \tag{79}$$

where

$$L_2 \equiv \frac{1 - B\left(\frac{\sqrt{R_e r}}{z}\right)^{-2\gamma}}{1 + B\left(\frac{\sqrt{R_e r}}{z}\right)^{-2\gamma}} . \tag{79a}$$

There are still three constants to be determined, and three boundary conditions remain:

1. At $r = a$: $w_i = w_e$. That is,

$$\frac{8\,Az^3}{(a^2R_i + Az^2)^2} = \frac{2z}{R_e}\left(\frac{\gamma}{a}\right)^2 [1 - L_2{}^2(a)] . \tag{80}$$

2. At $r = a$: $v_i = v_e$, or

$$\frac{4a(Az^2 - a^2R_i)}{(a^2R_i + Az^2)^2} = \frac{2}{aR_e}[\gamma^2(1 - L_2{}^2) - (1 + \gamma L_2)] . \tag{81}$$

3. The momentum balance gives

$$2\int_0^a w_i{}^2 r dr + 2\frac{\rho_e}{\rho_i}\int_a^\infty w_e{}^2 r dr = \frac{4}{3} . \tag{82}$$

The constant $4/3$ is obtained by assuming that the velocity profile in the nozzle fits the parabolic form $1 - r^2$.

These three conditions are solved for γ^2 and $\gamma L_2(a)$; from these, γ and B are readily obtained. Thus, from Eqs. (80) and (81), we obtain

$$\gamma^2 = \frac{4a^2R_e}{(Az^2 + a^2R_i)}\left(\frac{Az^2 + a^2R_e}{Az^2 + a^2R_i} - 1\right) + 1 , \tag{83}$$

$$\gamma L_2(a) = \frac{2a^2 R_e}{Ax^2 + a^2 R_i} - 1 . \tag{84}$$

The third equation then involves A as the only unknown. The first integral of the momentum balance may be integrated analytically, but the second must be done numerically. In this study, Simpson's rule was used to evaluate the second integral on an IBM 7090 computer. In most cases a fairly good approximation of the momentum balance was obtained by integrating the first integral from zero to infinity:

$$\frac{4}{3} = 2 \int_0^\infty \left[\frac{8\ Az^2}{(Az^2 + r^2 R_i)^2} \right]^2 rdr , \tag{85}$$

from which we get

$$A = \frac{16}{R_i} . \tag{86}$$

However, for two cases studied experimentally, this approximation was not good enough. In those cases Eq. (85) had to be divided into two separate terms as indicated in boundary condition 6. The two cases involved (water-n-heptane and water-isoamyl alcohol) were for liquid pairs with viscosities that were very different.

The jet radius can also be calculated, as a function of z, from the material balance:

$$1 = 2 \int_0^a w_i rdr . \tag{87}$$

Integration gives

$$a^2 = \frac{Az^2}{8z - R_i} . \tag{88}$$

In fact the jet begins for $a = 1$; i.e., this is the point where we wish to truncate the solution. Solving for z at this point, we get

$$z_0 = \frac{8 \pm \sqrt{64 - 4AR_i}}{2A} .$$

Then, since $A = 16/R_i$, we obtain

$$z_0 = \frac{R_i}{4} . \tag{89}$$

2. Exponential Method

For immiscible liquid-liquid jets, the Schlicting method appears deficient in two aspects. First, the continuous-stress criterion cannot be satisfied at the interface between the two liquids. Second, as observed experimentally, the jet decreases in area for a distance after leaving the orifice, before it begins to expand; whereas the Schlicting-type solution, which gives a continuously expanding jet, only applies beyond the point where the jet has reached its minimum cross-sectional area.

It appeared that these objections could be overcome, at least partly, by assuming an equation for the velocity distribution and then making it fit certain conditions. The empirical forms of velocity profile chosen for the jet and for the outside phase are

$$w_i = A\, e^{-mz/R_i}\, e^{-Br^2} , \tag{90}$$

$$w_e = A'\, e^{-B'r^2} . \tag{91}$$

Here A must have a value near 2.0, by comparison with a parabolic velocity profile. The nine required conditions are:

1. $r = 0: \quad \dfrac{\partial w_i}{\partial r} = 0 ,$

2. $r = 0: \quad w_i \dfrac{\partial w_i}{\partial z} = \dfrac{1}{R_i}\left(\dfrac{1}{r}\dfrac{\partial w_i}{\partial r} + \dfrac{\partial^2 w_i}{\partial r^2}\right),$

3. $r = a: \quad w_i = w_e ,$

4. $r = a: \quad \mu_i \dfrac{\partial w_i}{\partial r} = \mu_e \dfrac{\partial w_e}{\partial r}$

(neglecting the divergence of the jet shape),

5. Mass balance, as in Eq. (87),

6. Momentum balance, as in Eq. (82),

7. $r \to \infty: \quad w_e \to 0 ,$

8. $z \to 0: \quad r = a_0 ,$

9. $z \to 0: \quad (w_i)_{max} = 2 .$

Several of these conditions are satisfied automatically, due to the choice of function for the profile. Conditions 2 through 6 remain, to determine the parameters m, B, A', B', and a; thus we have five equations and five unknowns. These are:

2a. $\dfrac{m}{2} e^{-mz/R_i} = B ,$

3a. $A e^{-mz/R_i} e^{-Ba^2} = A' e^{-B'a^2} ,$

4a. $B' = (\mu_i/\mu_e)B ,$

$$5a. \quad 1 = \frac{Ae^{-mz/R_i}}{B}\left(1 - e^{-Ba^2}\right),$$

$$6a. \quad \frac{4}{3} = \frac{Ae^{-2mz/R_i}}{B}\left(1 - e^{-2Ba^2}\right) + \frac{\rho_e}{\rho_i}\,\frac{AA'^2}{4B'}\,e^{-2B'a^2}.$$

From these five equations, we find that m must satisfy the following equation:

$$1 = \frac{3A}{2m}\,e^{-mz/R_i}\left[1 - \left(1 - \frac{\alpha A^2}{4}\right)\left(1 - \frac{m}{2A}\right)^2\right], \tag{92}$$

with

$$\alpha \equiv \frac{\rho_e \mu_e}{\rho_i \mu_i}. \tag{93}$$

Based on an assumed value of A (e.g., $A = 2$), Eq. (92) can be solved numerically for m as a function of α and z/R_i, with the aid of a computer. Alternatively, an explicit solution can be obtained for z/R_i, and this can be plotted as in Fig. 6. After m is calculated, the other four parameters are solved for explicitly, as follows:

$$B = \frac{m}{2}\,e^{-mz/R_i}, \tag{94}$$

$$B' = (\mu_i/\mu_e)B, \tag{95}$$

$$A' = A\,e^{-mz/R_i}\,e^{-a^2(B-B')}, \tag{96}$$

$$a^2 = \frac{-\ln\left[1 - (B/A)e^{mz/R_i}\right]}{B}. \tag{97}$$

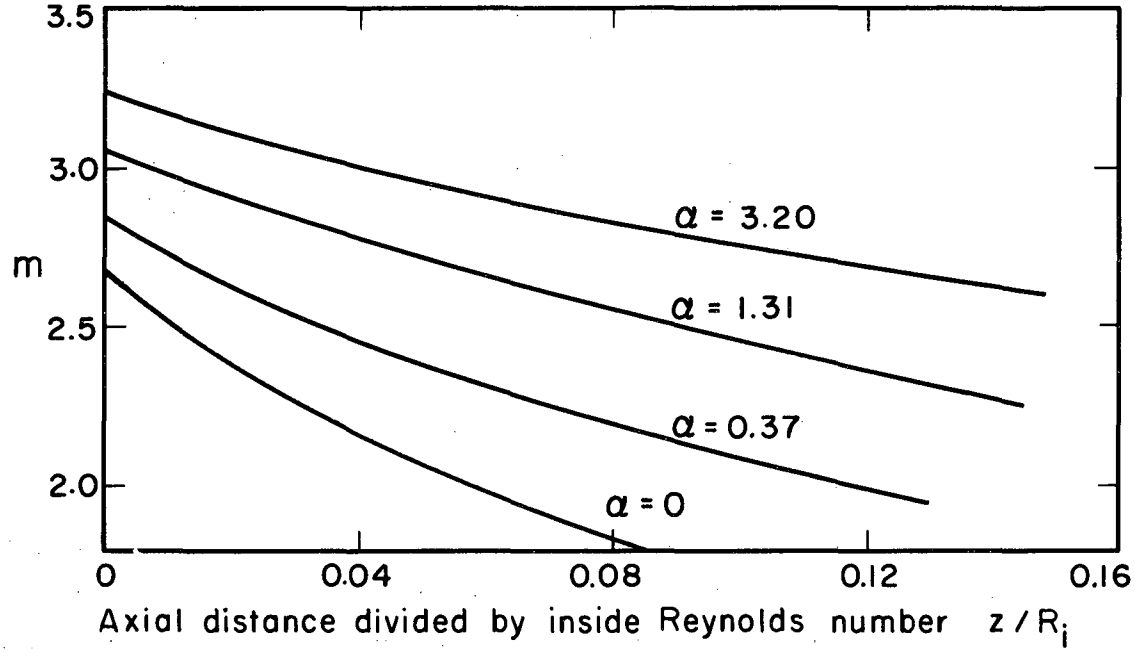

MU-29596

Fig. 6. Center-line velocity parameter as a function of jet length and density-viscosity product ratio.

In the present study, $A = 2$ has been used throughout. This is relatively precise at $\alpha = 1$. For α values greatly different from 1, a somewhat better fit to the mass balance would be given by using the relation $A = (7/4) + 5\alpha/(4\alpha + 16)$. The basic problem is that Eqs. (90) and (91) do not describe the jet exactly at the nozzle $(z = 0)$, even though they give a much better fit there than Eq. (62).

The behavior of these equations at $\alpha = 0$, corresponding to a liquid jet in air, is of interest for reference. Equation (92) then simplifies to:

$$\frac{z}{R_i} = \frac{\ln[3(4A - m)/8A]}{m} . \tag{98}$$

At $z = 0$, then, $m = 4A/3$. At large z, mz/R_i approaches the constant value of $\ln 1.5$ (= 0.406).

In the preceding analysis we have treated m as a constant. Strictly speaking this is not correct, but it is a good approximation. A rigorous mathematical treatment would be handled in the following manner. Let the velocity profiles, replacing Eqs. (90) and (91), be given by

$$w_i = 2F_1(z)\, e^{-Br^2} , \tag{99}$$

$$w_e = F_2(z)\, e^{-B'r^2} . \tag{100}$$

After introducing all of the required conditions, we would obtain the following equation for $F_1(z)$:

$$\frac{1}{3} = -\frac{F_1^{\,2}(z)}{F_1'(z)R_i}\left[1 - (1 - \alpha)\left(1 + \frac{F_1'(z)R_i}{4F_1(z)}\right)^2\right], \tag{101}$$

$$F_1'(z) = \frac{dF_1(z)}{dz} . \tag{102}$$

This equation is nonlinear, and would have to be solved numerically. This did not seem necessary, since we could obtain a good approximation by setting

$$F_1(z) = e^{-mz/R_i}, \tag{103}$$

as was done in Eqs. (90) and (91). The approximation enters into condition 2. The exact form is

$$\frac{1}{2} e^{-mz/R_i} \left(m + z \frac{dm}{dz} \right),$$

and the term that has been neglected is

$$z \frac{dm}{dz}.$$

This term does not become appreciable until z reaches a value larger than 100. In the present experiments, such high values of z are never involved, hence the approximation used here is adequate.

As already shown, m can be plotted as a function of z, R_i ($= c\, a_0\, \rho_i/\mu_i$), and α ($= \rho_e\, \mu_e/\rho_i\, \mu_i$). By use of Eqs. (94) through (97), B is found from m, z, and R_i; and a from B, m, z, and R_i. Through m, then, the inside-phase parameters B and a are each a function only of z/R_i and of α; these relations (based on $A = 2$) are shown in Figs. 7 and 8. If the outside profile is desired, B' is calculated from B, μ_i, and μ_e; and A' from the other parameters, by Eq. (96).

Figure 9 is a graph of jet radius, interface velocity, and center-line velocity, as functions of z for a typical system. Like Fig. 8 this gives a somewhat pictorial representation of the change in diameter of the jet.

Figures 10, 11, and 12 give comparisons of the Schlichting and exponential methods for three different liquid-liquid systems, each

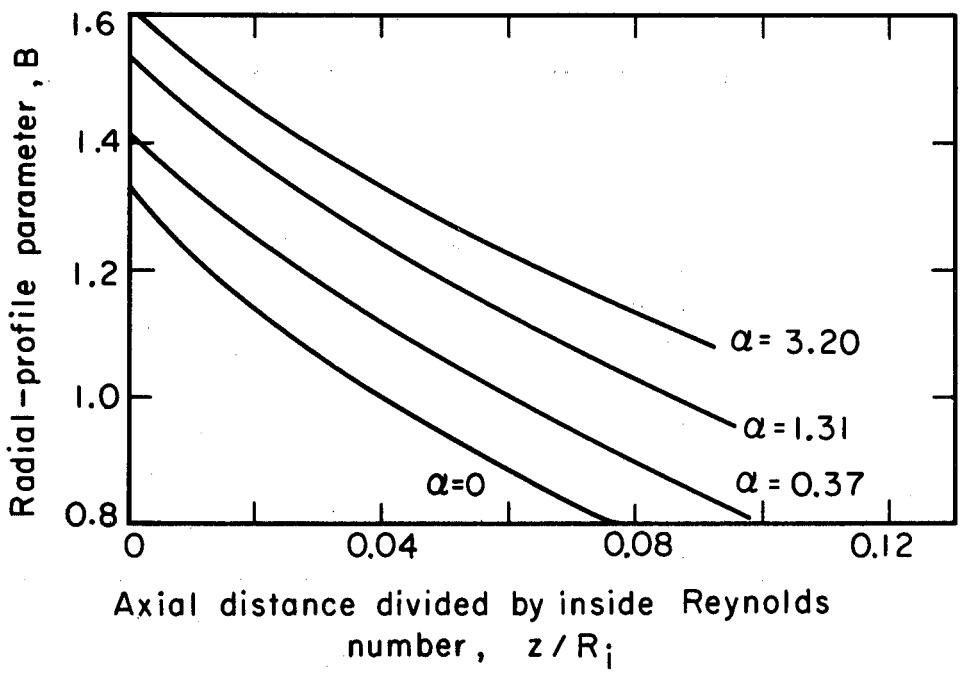

Fig. 7. Radial parameter of the axial velocity as a function of jet length and density-viscosity product ratio.

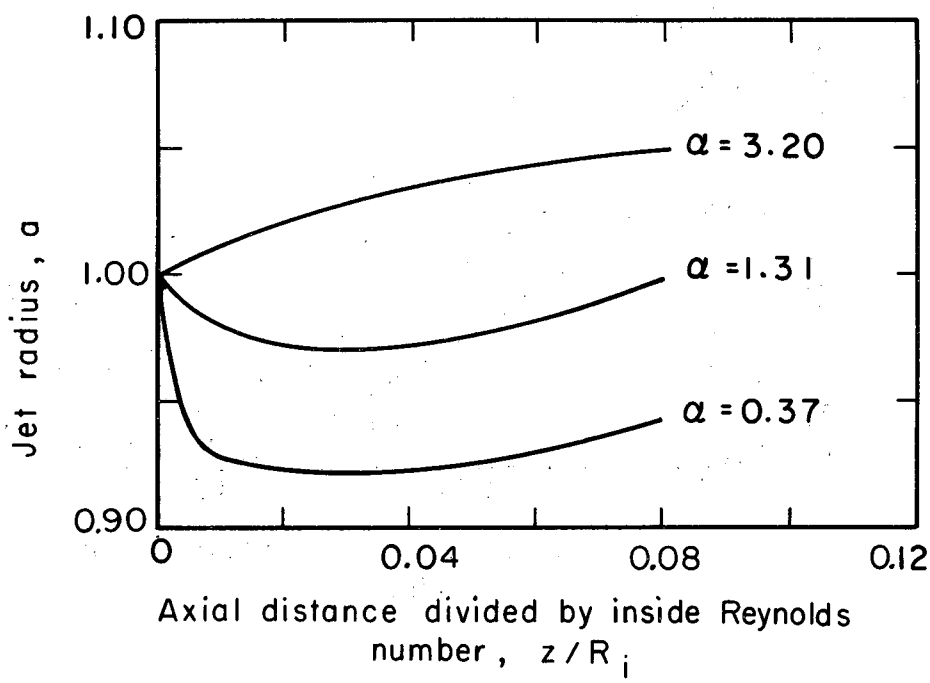

MU-29954

Fig. 8. Jet radius as a function of jet length and density-viscosity product ratio.

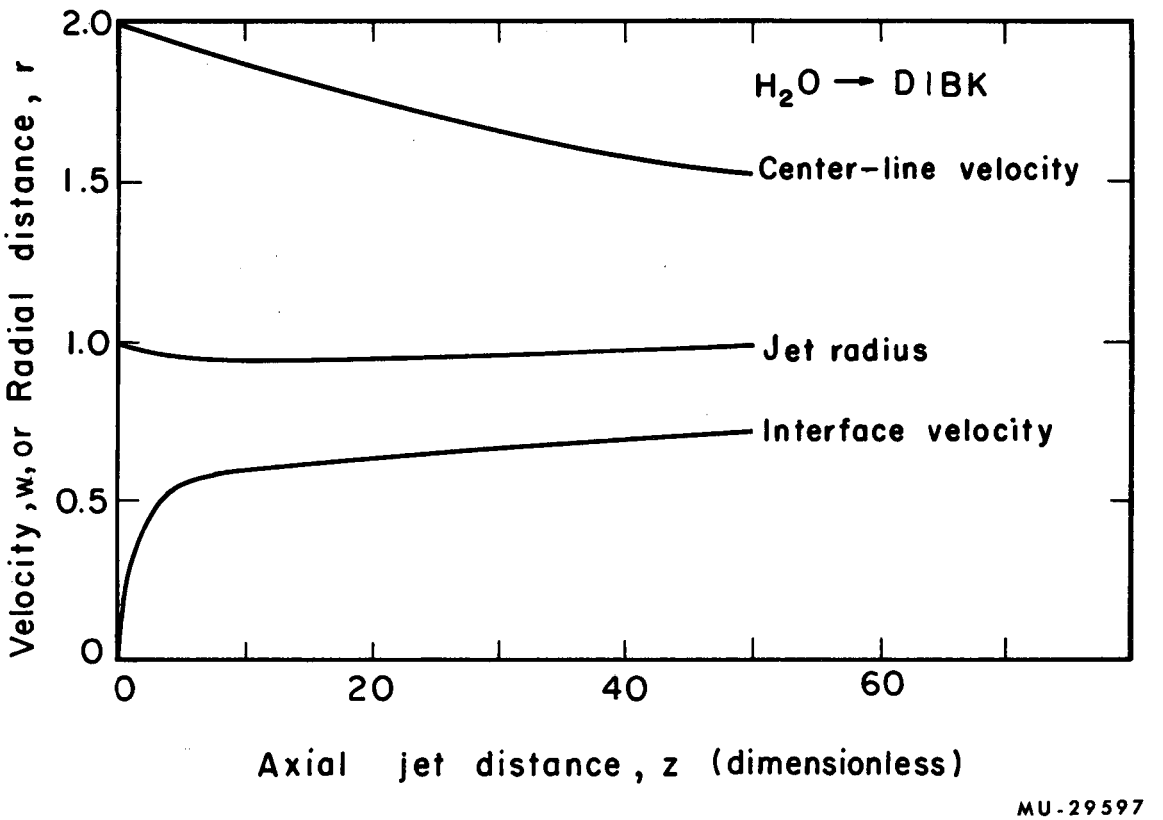

Fig. 9. Center-line and interface velocity and jet radius as function of jet length (α = 0.74).

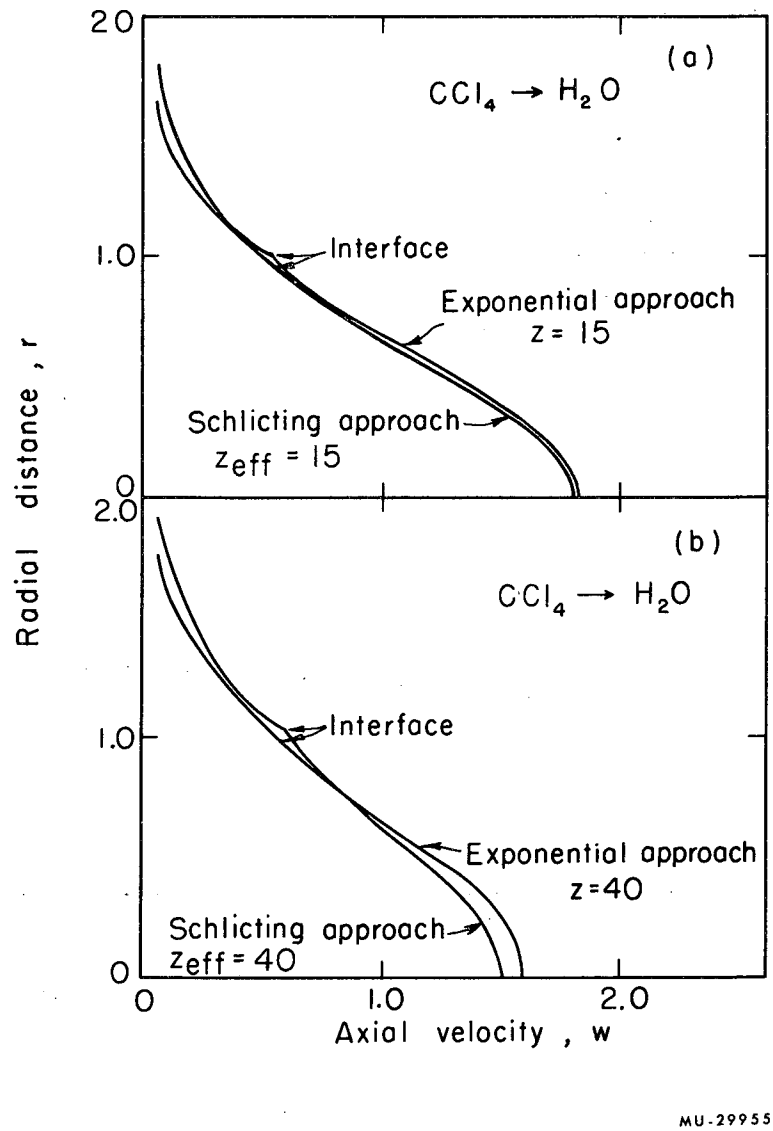

Fig. 10. Comparison of exponential and Schlicting-type velocity profiles; carbon tetrachloride into water; (a) z = 15, (b) z = 40.

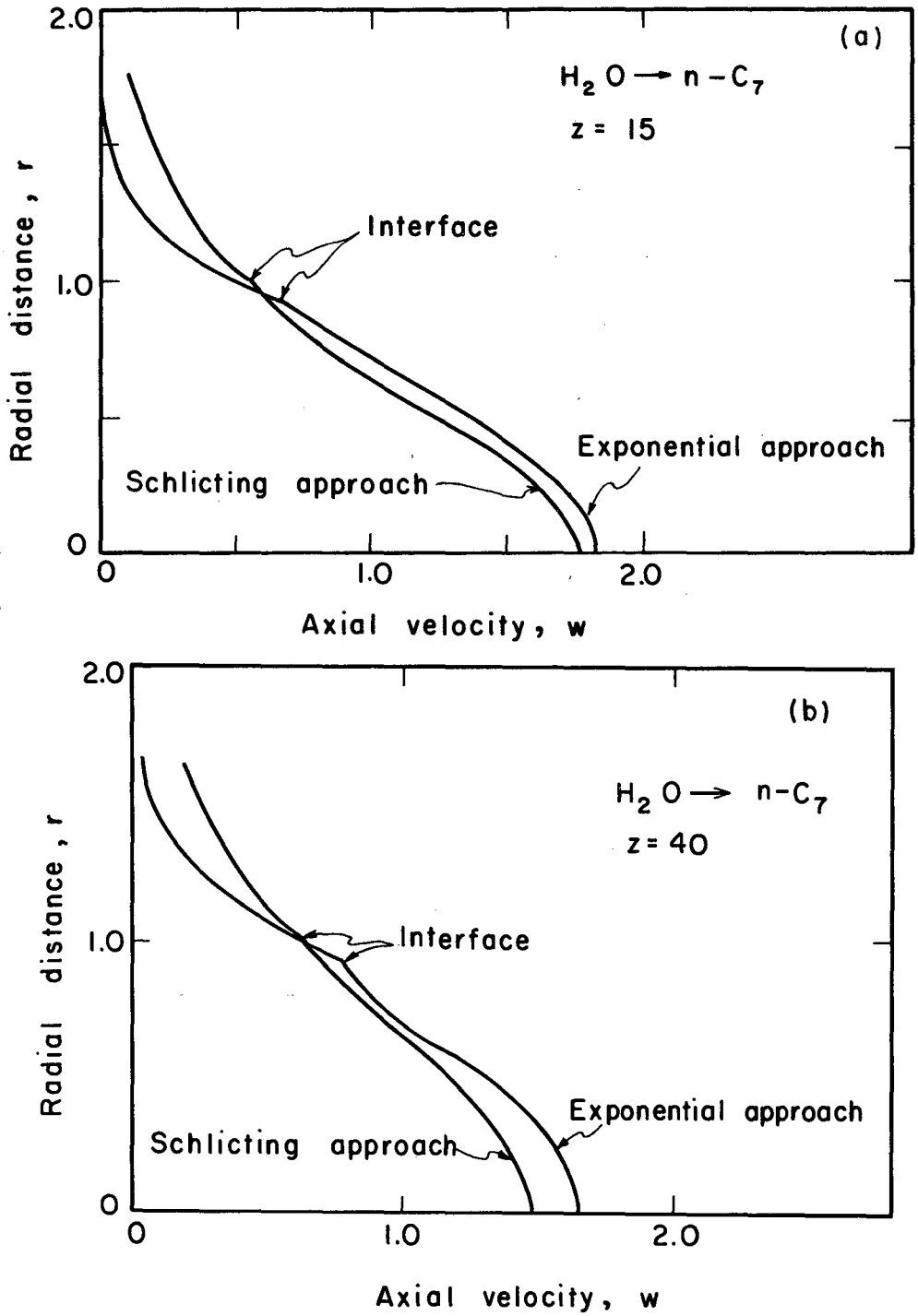

MUB-1677

Fig. 11. Comparison of exponential and Schlicting-type velocity profiles; water into normal heptane; (a) z = 15, (b) z = 40.

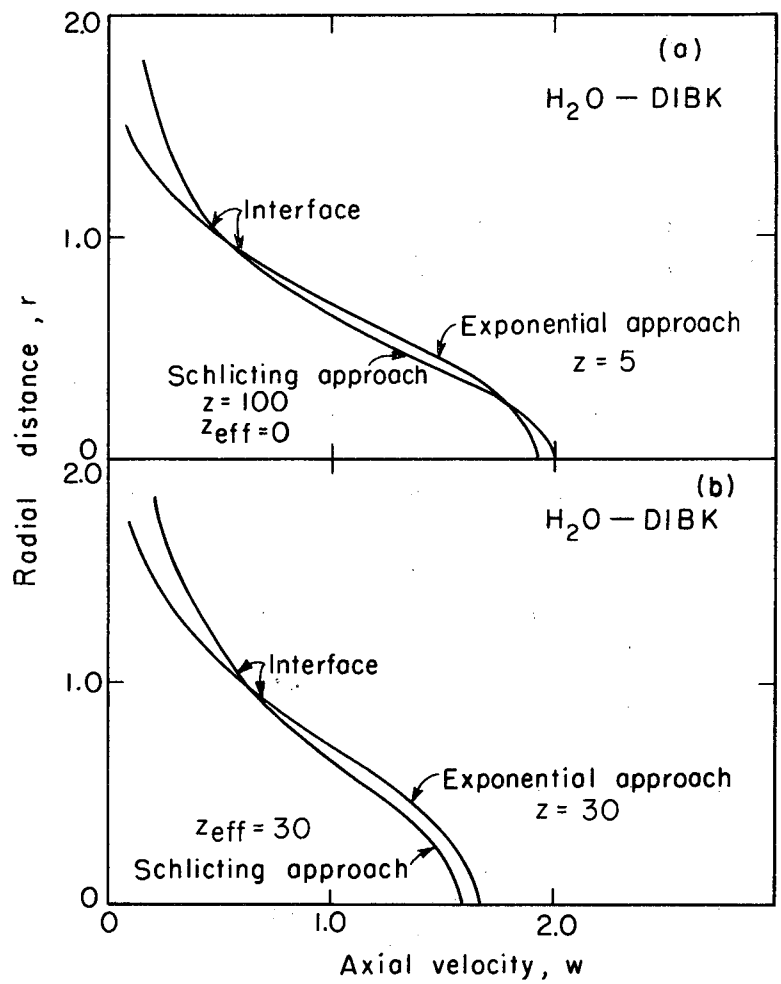

Fig. 12. Comparison of exponential and Schlicting-type velocity profiles; water into di-isobutyl ketone; (a) z = 5, z(eff) = 0, (b) z = 30.

shown at two values of z. As indicated earlier, the procedure for fitting the Schlichting-type result to the true jet is somewhat arbitrary. It is possible that a different procedure would cause the Schlichting-method curves to correspond more closely to a true jet (and also, probably, to the exponential-method curves).

IV. EXPERIMENTAL STUDY

A. Apparatus and Measurements

From the theoretical analysis, it is seen that the quantities that must be measured from an oscillating jet in order to calculate the interfacial tension are: the wavelength of the oscillations, the jet flow rate, the maximum and minimum diameters of the jet at the place of measurement, and the densities and viscosities of the two liquids.

A schematic diagram of the flow system used to obtain the jet measurements is shown in Fig. 13. It consists of a feed reservoir that provides constant flow, polyethylene tubing with regulatory valves, a rotameter, and a jet chamber. A photograph of the jet chamber, $4 \times 4 \times 12$ in., constructed of lucite acrylic polymer slabs, is shown in Fig. 14. The constant-flow reservoir is similar to one used by Defay and Hommelen.[16] The valve in the line ahead of the nozzle allows for varying the flow rate without moving the reservoir.

B. Materials

During an experimental run—in order to avoid any mass-transfer or adsorption—the phases were mutually saturated before the start of the run. The liquids that were used in the experiments were di-isobutyl ketone ("DIBK"), cumene (isopropyl benzene), normal heptane, carbon tetrachloride, isoamyl alcohol, and water. Water was always taken as one phase, and an organic compound as the other. The cumene and n-heptane were from Phillips Petroleum Company and were technical grade (with less than 5 % impurity, of similar chemical nature). The DIBK, from Union Carbide Chemical Corp., also had a purity of at least 95 %. The carbon tetrachloride and isoamyl alcohol, from Allied Chemical Corp., were 99+ % pure.

C. Physical Properties

Viscosities were found with an Ostwald viscometer, calibrated with water. Density measurements were made with a pycnometer, also

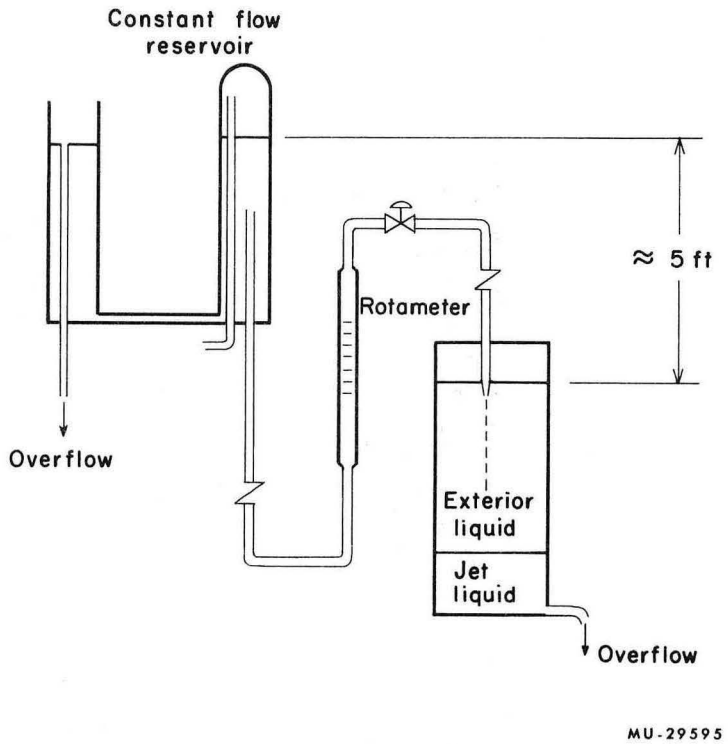

Fig. 13. Flow diagram.

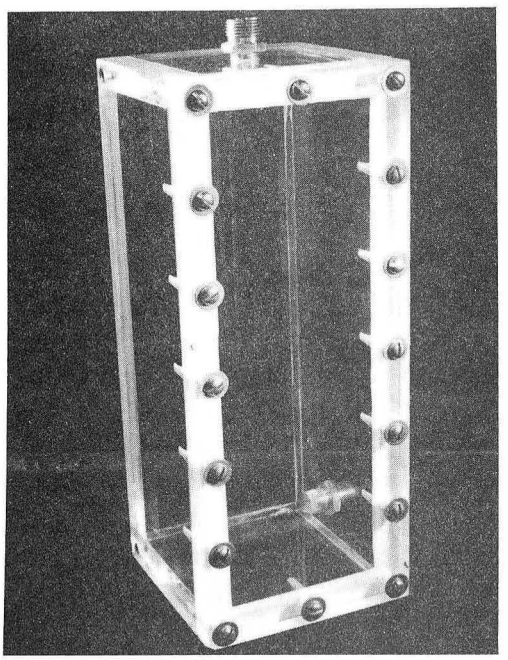

ZN-3635

Fig. 14. Unpainted jet chamber.

calibrated with water. The interfacial tension was checked before and after each run with a Du Nouy ring tensiometer. This was done to make sure no contamination had taken place during the run, and also to provide a standard for the oscillating-jet method. The properties of the liquids used are given in Table I.

Table I. Physical properties of liquid used.

Compound	Density (g/cm^3)	Viscosity (g/cm-sec)	Interfacial tension against water (25°C) (dyn/cm)
Water	1.00	0.0091	--
Cumene	0.86	0.0080	35.6
n-Heptane	0.68	0.0049	42.2
Carbon tetrachloride	1.59	0.0091	41.4
Di-isobutyl ketone	0.81	0.0086	21.5
Isoamyl alcohol	0.81	0.0360	6.1

D. Optics

The wavelength and the maximum and minimum diameters of the jet were measured photographically. The illumination assembly and the camera location are shown in Fig. 15.

The method most frequently used to measure wavelength is due to Stocker.[31] This method utilizes the fact that the waves will act as cylindrical converging lenses when parallel light is passed through the stream perpendicular to its axis. The light converges into a series of parallel lines, each located at a node of the wave pattern, that may be focused on a photographic plate. The distance between two adjacent lines is thus the wavelength.

Stocker's method is convenient and accurate. However, it cannot be used in most liquid-liquid systems, because the convergence or divergence of a lens depends partly on the refractive indexes of the lens

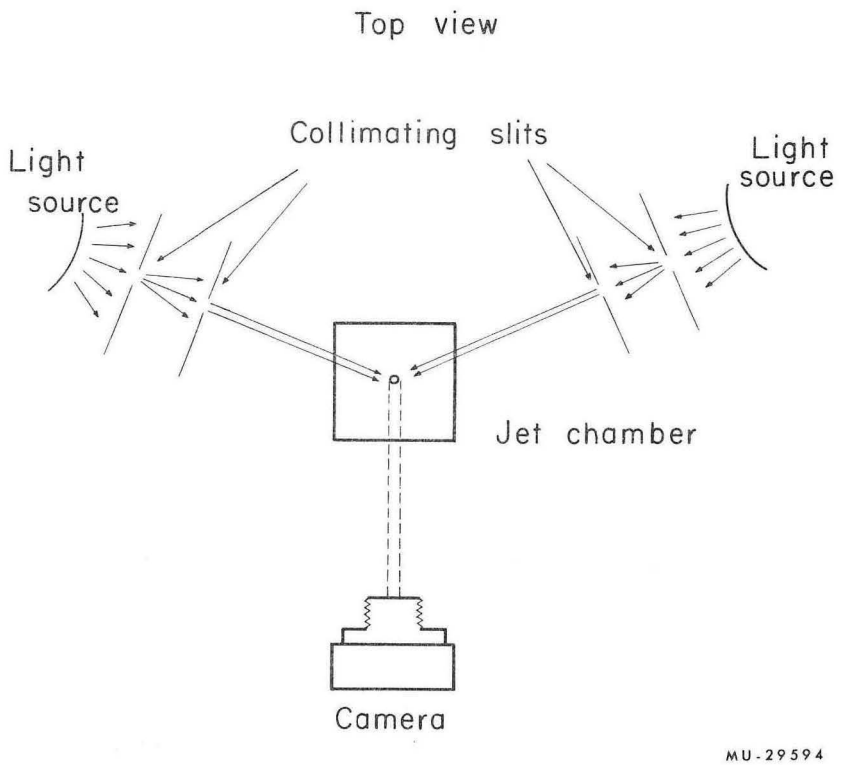

Fig. 15. Illumination diagram with camera position.

and the medium surrounding the lens. In gas-liquid systems the liquid always has a substantially higher index of refraction, and the stream will act as a converging lens. In liquid-liquid systems, the jet liquid may easily have a lower index of refraction than the exterior liquid, and in this case the jet acts as a diverging lens. Even when the jet does have a higher refractive index than the outside phase, the difference in refractive index is small enough so that the focal length of the wave is generally too long for practical measurements.

The method used in the present experiments has an advantage over Stocker's method in allowing both wavelength and diameter measurements to be made from a single experiment. Its disadvantages are that the jet is much more difficult to illuminate properly, and that the measurements made on the negative are much less accurate than those using Stocker's method.

One difficulty in obtaining proper illumination of the jet was caused by reflections from the inner surfaces of the Lucite walls of the containing vessel. To help overcome this problem, the jet was illuminated from both sides, so that the light on the jet was distributed symmetrically. In order to remove a part of the reflection, the outside of the container was painted a dull black, except for four small windows. The inside could not be coated because it would have contaminated the system. A photograph of the coated container is shown in Fig. 16.

The photographs of the jet were taken with a 135-mm Pacemaker Graphic camera, using a Graflex Optar lens fitted with accessory lenses giving a correction of four diopters. The photographic plate was generally positioned 10 to 12 in. from the stream, and gave a magnification of about 2X. The nozzle, which had accurately known dimensions, was used to determine the exact magnification ratio; a scale factor, calculated from the nozzle for each photograph, was used to adjust the measured values for the wavelength and diameters.

The nozzles were calibrated with a Nikon model-3A Optical Comparator accurate to 0.0001 in. The actual wavelength measurements from the photographic negative were made with a Vanguard Motion Analyzer which was accurate to 0.001 in.; with this machine a

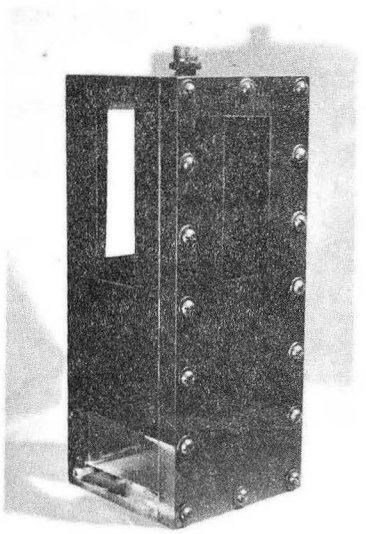

ZN-3636

Fig. 16. Painted jet chamber.

further magnification of from 2.5× to 16× could have been obtained, and a ratio of 4× was generally used. The limitation to this method lies in the difficulty of determining the exact maximum or minimum of the wave. For this reason the accuracy of the wavelength and diameter measurements is only ±0.005 in. (in actual length), which amounts to approximately ±2 to 5%.

Figure 17 is an example of one of the photographs that was measured. This particular photograph is of a jet of water directed into di-isobutyl ketone.

E. Preparation of Nozzles

One of the more difficult problems encountered when the oscillating jet is used is the preparation of the elliptical nozzle. Several different methods of preparing these nozzles have been used,[1-6,16-18,21-23] most of which have been tried in the course of the present work. The best-known method for making liquid-gas nozzles, by sagging of glass capillaries in a furnace, was found not to be best for liquid-liquid nozzles. For the latter, the best nozzles could be made by heating glass capillary tubing in a flame, drawing it to obtain a taper, pressing the tip between flat graphite plates to form an elliptical cross section, and then removing part of the tip.

It is very important that the nozzle be broken off squarely after it has been pressed, in order to obtain a very sharp well-defined edge. Cutting the nozzle with a glass-saw produces scratches in the rim of the opening which will affect the jets adversely.

Several other methods of making the nozzles were tried. The points on stainless-steel hypodermic needles were ground flat and pressed into elliptical shapes. These were found unsatisfactory because they frequently split during pressing, or they contained burrs in the opening, from the grinding. Among various glass companies contacted for possible manufacture of nozzles, most would not attempt to make them; one company that did try was not very successful. We also tried to form glass around an elliptical mandril, but then had the problem of preparing the mandril, which was not solved adequately.

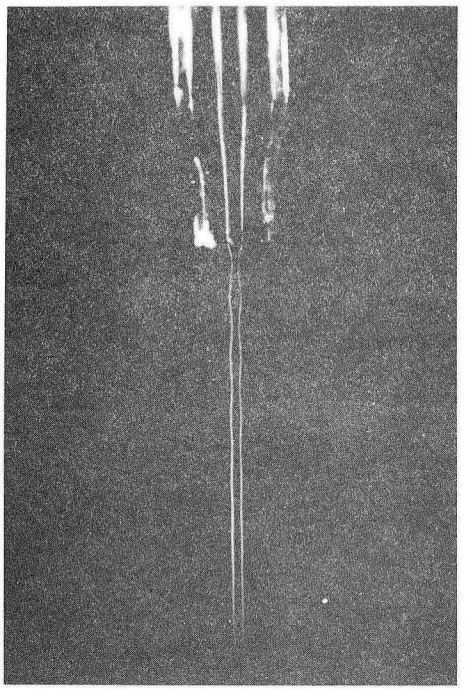

ZN-3637

Fig. 17. Picture of an oscillating jet.

In regard to the length of nozzle required, we found that because of the small-diameter tubing being used, the nozzles could be as short as 1.5 in. without having problems caused by incompletely developed velocity profiles at the nozzle outlet. Many nozzles had to be made before even a few acceptable ones could be obtained. Out of 350 trials, 20 nozzles gave a passable performance, and six were selected for more extensive use. The dimensions of these final six are given in Table II. Figure 18 is a photograph of three of the nozzles.

Table II. Jet dimensions.

Jet No.	Max diam (cm)	Min diam (cm)	Area (cm^2)
1	0.109	0.061	0.00519
2	0.100	0.055	0.00434
3	0.108	0.061	0.00517
4	0.166	0.059	0.00767
5	0.139	0.064	0.00703
6	0.196	0.066	0.0102

F. Measurements

A few generalizations should be made here about the oscillating jets encountered in the present experiments.

First, as the theory would predict, the wavelength of the jet depends very strongly on the velocity and the interfacial tension. When the jet velocity was decreased, more waves—which were each shorter—became visible. A still further decrease caused the waves to blur and disappear, giving a cylindrical jet with a diameter near that of the equivalent diameter of the nozzle. At the maximum velocity used, only about one-half wavelength remained visible before the jet broke up into droplets. Runs were generally made at or near the velocity at which the greatest number of waves was visible, and at one or two higher velocities.

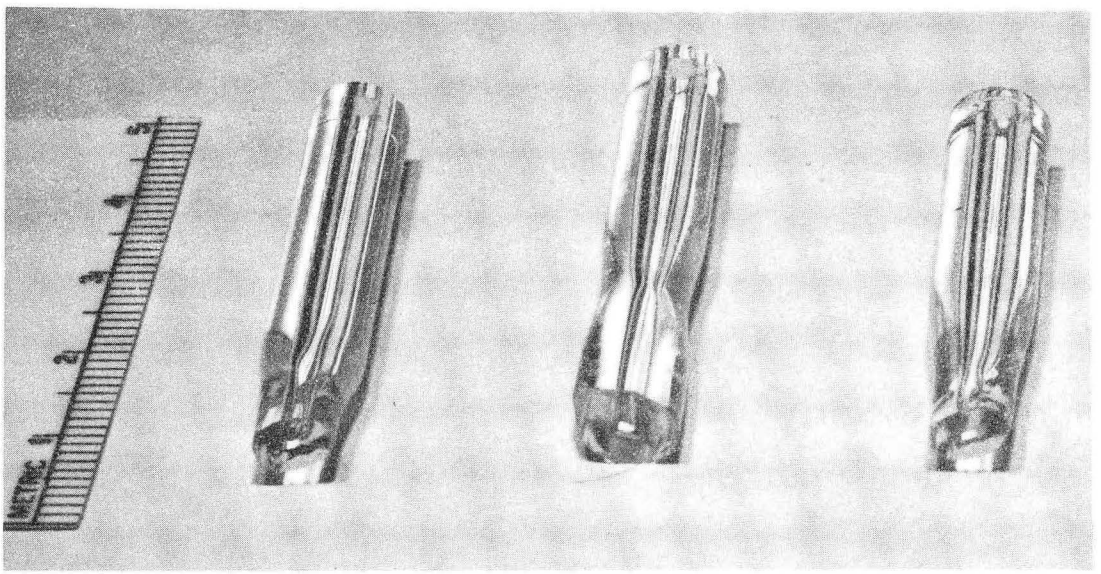

ZN-3638

Fig. 18. Three elliptical nozzles.

Second, for three of the jets there was an unexpected and unwanted variation in the wavelength. Nozzles 4 and 6 gave jets whose wavelengths increased steadily with increasing flow rates, in the operable range. Nozzle 5 also showed some variation in wavelength behavior, less pronounced than for nozzles 4 and 6. These three nozzles had the largest cross sections and the greatest eccentricities, and did not conform as closely to the required mathematical ellipse as jets 1, 2, and 3. For this reason only one run was made with nozzles 4 and 6; nozzle 5 was used more frequently. Any variations in the wavelength of jets from nozzles 1, 2, and 3 can probably be attributed to the finite distance required to dissipate the nozzle's effects on the velocity profile.

The third generalization is that it is possible to use either the more- or less-dense liquid as the jet phase. Two of the systems used were run successfully both ways: di-isobutyl ketone - water, and cumene - water. Carbon tetrachloride - water and n-heptane - water were both tried also, but with poorer results. Isoamyl alcohol as the jet liquid was not tried. When the less-dense liquid is the jet phase, the jet is directed vertically upward. The opposite is true with the more-dense liquid as the jet phase. Gravity played no measurable part in lengthening or shortening the wavelengths.

The data are presented in Appendix A. The jet liquid is always named first. Experiment 2, water into cumene, is not presented, because it was found that the cumene from one of the containers was contaminated with resinous particles. The scale-correction factor includes only the conversions to account for magnifications and put the final values into the proper dimensions. The velocity given is the mean velocity of the jet as it leaves the nozzle (flow rate divided by nozzle cross-sectional area). The first value given in the maximum-diameter column for each experiment is the maximum diameter of the nozzle. The wavelengths were measured from minimum to minimum, and thus the first half wavelength is not included.

V. DISCUSSION

Table III gives a comparison of the calculated and actual values of the interfacial tension for the nine experiments that were carried out. The scatter of the calculated value is very often high, and off by more than 50% in some cases. However, the values in all but very few of the 70 or 80 experiments are within 25% of the correct value, which is moderately good when the wide range of interfacial tensions used is considered. The results are somewhat better for those experiments (Nos. 3, 4, 5, and 10) in which it was possible to obtain four or more waves. These were water into di-isobutyl ketone, carbon tetrachloride into water, water into cumene, and water into isoamyl alcohol. The last system gave only about 2.5 waves; however, because of the extremely low interfacial tension, its long wavelength gave jets as long as the others, and it could be measured with higher accuracy.

Where the less dense liquid was used for the jet, it was possible in two systems to obtain four wavelengths. These were di-isobutyl ketone into water, and cumene into water. In these cases, the jets were much more unstable than in the reverse cases; that is, more susceptible to breakup by a random shock. They were also variable, and seemed to give better jets on one day than another.

Our being able to obtain data from systems where the less-dense liquid was the jet phase constitutes an improvement over the only previous work with liquid-liquid systems. In Addison's experiments[1-6] using the less-dense liquid as jet phase, the jets broke up before the end of the first node. However, he obtained as many as ten nodes when directing CCl_4 into water, whereas we were able to get only five or six in this system. Our inability to get longer jets suggests that the scatter in our interfacial-tension values is largely due to our not having had good enough nozzles.

There seems to be a density factor not accounted for by our present mathematical treatment. As seen from the data, when the more-dense liquid is the jet phase, the calculated values are always too low; for the reverse case, the values are too high. It is possible

Table III. Comparison of actual and calculated values of interfacial tension.

Run	σ calc.	σ actual	Run	σ calc.	σ actual
1-b	55.5	42.2	6-a	5.2	6.1
c	70.1		b	5.5	
d	63.8		c	4.2	
e	41.8		d	3.5	
g	45.0		e	4.6	
h	35.5		g	4.8	
k	39.1		h	7.2	
l	32.7		k	10.5	
m	66.0				
n	34.2		7-a	23.3	21.5
o	50.5		b	37.5	
			c	45.8	
3-a	16.8	21.5	d	19.3	
b	17.5		e	42.5	
c	18.0		f	37.8	
d	17.2		g	25.6	
e	14.0		h	28.8	
f	13.7		k	33.2	
g	18.1		l	41.5	
h	18.0				
l	15.6		9-a	71.0	35.6
k	17.7		b	53.0	
m	14.5		c	27.5	
n	14.8		d	45.6	
			e	40.4	
4-a	36.5	41.4	f	45.0	
b	49.2		g	30.3	
c	50.0		h	40.4	
d	49.5		k	50.8	
5-a	31.4	41.4	10-a	33.2	35.6
b	33.4		c	45.2	
d	29.5		b	33.5	
e	39.1		d	30.4	
g	35.3		e	33.3	
k	39.2		f	33.2	
h	50.5		g	42.7	
			h	45.3	
			k	45.5	

to get a rough correction by plotting the actual value divided by the calculated value vs the density ratio. This plot was made in Fig. 19, using only what appeared to be our most reliable data, and these data do little more than suggest a trend.

Another very important factor to be considered is that the nozzles used do not fit exactly the mathematical form of an ellipse. This has led other investigators[16-18] to conclude that each nozzle gives a wavelength that must be corrected for the nozzle's deviation from an ellipse. Defay and Hommelen used water as a standard to find the correction factor for each jet. The deviation of our nozzles is probably larger than that of Defay and Hommelen, because more-eccentric nozzles are needed to make visible waves in the liquid-liquid systems.

Of the four nozzles plotted, three seem to form a family of parallel lines. One would expect the lines to be parallel or concurrent in one point with the correction factor due to the imperfection of the ellipse as a parameter that would collapse all of the lines into one line. Table IV gives several of the best runs with this correction.

In order to develop this method of measuring interfacial tension into a more useful tool, there are four areas in which more work is necessary. First, better nozzles are needed. From the present work we have seen that at least four waves are necessary for the results to be fairly reliable. (When mass transfer is to be measured, a larger number yet will be needed.) To improve the jets it is necessary to find a method of making a nozzle with a more perfect ellipse, but still with relatively high eccentricity. The most promising method still untried is probably that of making a metal mandril around which the nozzle can be formed. One way to make it would be from an elliptical die, through which a wire could be drawn to give the desired shape.

Second, it is definitely possible to improve the illumination of the jet. This can be done by using lenses to focus the light, along with the collimating slits that were used in the present work. The thinner the band of light that illuminates the edge of the jet, the more accurate the measurements of wavelength and jet diameter will be. Another possible improvement would be the building-in of a cylindrical lens, inside the jet chamber or as part of the chamber wall.

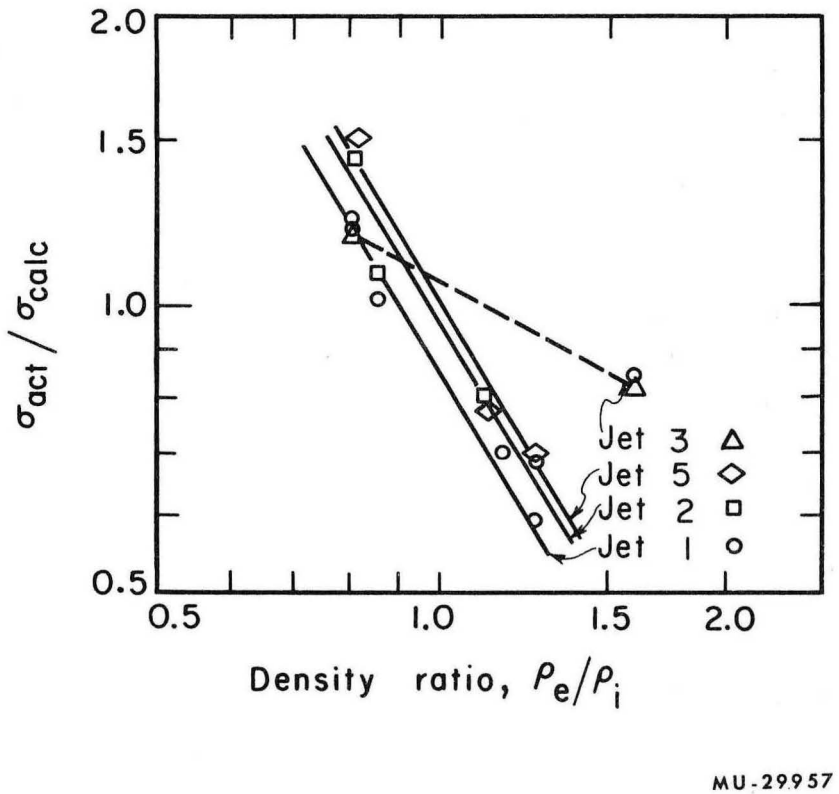

Fig. 19. Empirical density correction.

Table IV. Comparison of corrected values of interfacial tension.

Run	Correction	σ^a	σ actual	Run	Correction	σ^a	σ actual
3-a	1.2	20.2	21.5	9-a	0.68	48.0	35.6
b		21.0		b		36.0	
c		21.6		c		19.0	
d	1.45	25.0		d	0.82	37.4	
e		20.3		e		33.2	
f		19.9		f		36.8	
g	1.2	21.7		g	0.80	24.0	
h		21.6		h		32.3	
l	1.45	22.6		k		41.4	
k	1.2	21.3					
m	1.45	21.0		10-a	1.10	36.5	35.6
n		21.5		c		49.6	
				b		36.8	
6-a	1.2	6.2	6.1	d	1.3	39.5	
b		6.6		e		42.3	
c		5.0		f		42.2	
d	1.45	5.1		g	1.3	50.0	
e		6.6		h		50.0	
g		6.9		k		50.0	
h	1.45	7.0					
k		7.0					

[a] Corrected.

Third, another new phase for experimental investigation would be the use of a flowing external phase (instead of a stationary one) at a velocity near the mean velocity of the jet fluid. The mathematical framework already developed would apply equally well to this case.

Fourth, the mathematical model for oscillation of the jet might be made more realistic with respect to axial-velocity distribution. This would make the differential equations much more difficult to solve, but numerical solution might still be possible. With this improvement, the mathematical model should take into account all possible variables, with the exception of nozzle imperfections.

VI. CONCLUSIONS

1. A mathematical derivation given here makes it possible to calculate interfacial tension from an oscillating-jet experiment to within 25 to 50% of the correct value. For experiments that we feel are most reliable the calculated value is within 25%. The mathematics is divided into two parts. First, an interfacial-tension relation was obtained, assuming a constant velocity profile. Second, the velocity profile for a circular jet was calculated by using two different approximations. This second derivation was used to give a velocity correction for the interfacial-tension relation.

2. The best nozzles for liquid-liquid systems were made by drawing heated capillary glass tubing to obtain a taper and then pressing the tubing into an elliptical shape. An ellipse is necessary that has just enough eccentricity to give visible waves in liquid-liquid systems. Too large an eccentricity causes the wavelength of oscillation along the jet length to vary. We believe that better nozzles might be made by forming the glass around a mandril, made by drawing a metal wire through an elliptical die.

3. The jet can be run with either the more-dense or the less-dense liquid as the jet phase. However, the results were better when the more-dense liquid was the jet phase.

4. The jet illumination can be improved by using lenses, plus the collimating slits that were used in the present work, to focus a tiny line of light on each edge of the jet. The smaller this line of light is, the more accurately the photographs that are taken of the jet can be measured. The limit on how fine a line of light may be used depends on the speed of the camera used and on the sensitivity of the film.

ACKNOWLEDGMENT

Thanks are due Professor Simon Goren and Professor Andreas Acrivos for their invaluable aid and advice; and to Ione Maxwell for making numerous elliptical glass nozzles.

The work described was performed in the Lawrence Radiation Laboratory under the auspices of the U. S. Atomic Energy Commission.

NOMENCLATURE

Symbol	Definition
$A, A', A_1, A_2, B, B', B_1, B_2, C_1, C_2, C_3, C_4, Q$	Arbitrary constants that appear in the solutions of various differential equations.
a	Average jet radius
a_0	Average nozzle radius
b	Wave number
c	Average axial velocity
d	Relative wave number defined in Eq. (24).
d_i	d for interior phase
d_e	d for exterior phase
D	Determinant, Eq. (56)
D/Dt	Substantial derivative
$f(r)$	General function to represent pressure or velocity
$F_1(z), F_2(z)$	Generalized axial variable for circular jet
g	x-direction velocity
g_1	Relative velocity, defined by Eq. (7)
h	y-direction velocity
h_1	Relative velocity, defined by Eq. (7)
h	Modified stream function
h_i	h for interior liquid
h_e	h for exterior liquid
i	$\sqrt{-1}$
I_n	Modified Bessel function of first kind
k_i	Represents terms that multiply σ in Eq. (54)
K_n	Modified Bessel function of second kind
L_2	Simplified variable in velocity expression, Eq. (79a)
m	Arbitrary parameter, Eq. (90)

Symbol	Definition
n	Separation constant, Eq. (20)
P	Pressure
r	Radial component of cylindrical coordinates
r_i	Difference in major and minor axes of an ellipse
r_x	Sum of major and minor axes of an ellipse
R	Reynolds number, $a_0 w_0/\nu$
R_i	Interior R
R_e	Exterior R
R_1, R_2	Principle radii of curvature of a surface
u, v, w	Components of velocity in cylindrical coordinates
u_1, v_1, w_1	Relative velocity components, defined in Eq. (15)
w_0	Average axial velocity
x, y, z	Components of rectangular coordinates
x_{ij}	General term of determinant Eq. (56)
y	Dummy variable, Eqs. (7) through (74)

Greek Letters

α	Ratio of density-viscosity products, Eq. (93)
γ	Arbitrary constant
∇^2	Laplacian operator
ϵ	Wave-damping coefficient
ζ	Surface function, Eq. (43)
η	Similarity variable
θ	Component of cylindrical coordinates
μ	Dynamic viscosity
μ_i	Interior viscosity
μ_e	Exterior viscosity
ν	Kinematic viscosity, μ/ρ
ϕ	Stream function

Symbol	Definition
ρ	Density
ρ_i	Interior density
ρ_e	Exterior density
σ	Interfacial tension
ω	Axial-velocity perturbation
ω_1	Relative perturbation, Eq. (7)

APPENDIXES

A. Experimental Data

Experiment 1

System: Water — n-Heptane

Run	Correction factor	Jet No.	Max diam (cm)	Min diam (cm)	Wavelength (cm)	Flowrate (cm^3/sec)	Velocity (cm/sec)
b	0.348	1	0.109	0.061		0.995	192
			0.094	0.055	0.523		
			0.088	0.057	0.535		
c	0.346		0.109	0.061		0.780	150
			0.088	0.062	0.368		
			0.085	0.067	0.358		
			0.081	0.067	0.369		
			0.077	0.069	0.359		
d	0.332		0.109	0.061		0.645	124
			0.083	0.066	0.273		
			0.081	0.068	0.293		
			0.081	0.070	0.278		
					0.283		
e	0.325	2	0.100	0.055		0.625	144
			0.066	0.043	0.290		
			0.068	0.043	0.319		
			0.067	0.044	0.319		
			0.067	0.044	0.322		
g	0.300		0.100	0.055		0.840	194
			0.075	0.039	0.434		
			0.071	0.042	0.426		
h	0.318	4	0.166	0.059		0.630	82
			0.081	0.073	0.322		
			0.083	0.075	0.284		
				0.081	0.274		
k	0.330		0.166	0.059		0.735	96
			0.093	0.073	0.342		
			0.088	0.073	0.352		
			0.085	0.073	0.349		
				0.075			
l	0.325		0.166	0.059		0.855	111
			0.096	0.064	0.448		
			0.095	0.065	0.450		
				0.071			
m	0.299	2	0.100	0.055		0.600	138
			0.067	0.052	0.229		
			0.063	0.052	0.230		
				0.057			
n	0.310		0.100	0.055		0.505	116
			0.070	0.052	0.292		
			0.069	0.053	0.303		
			0.063	0.055	0.318		
				0.056	0.308		
o	0.312		0.100	0.055		0.935	192
			0.076	0.050	0.455		
			0.073	0.050	0.453		

Experiment 3

System: Water — DIBK

Run	Correction factor	Jet No.	Max diam (cm)	Min diam (cm)	Wavelength (cm)	Flowrate (cm^3/sec)	Velocity (cm/sec)
a	0.329	1	0.109	0.061			
			0.080	0.042	0.490	0.615	119
			0.075	0.049	0.500		
			0.072	0.054	0.500		
				0.056	0.500		
b	0.330		0.109	0.061			
			0.073	0.047	0.395	0.515	99
			0.073	0.052	0.404		
			0.072	0.053	0.406		
			0.071	0.055	0.408		
				0.055	0.406		
c	0.341		0.109	0.061			
			0.087	0.042	0.624	0.740	143
			0.083	0.048	0.629		
			0.076	0.056	0.632		
d	0.351	2	0.100	0.055			
			0.077	0.032	0.538	0.600	138
			0.077	0.038	0.560		
			0.076	0.046	0.558		
			0.074	0.049	0.548		
e	0.344		0.100	0.055			
			0.077	0.035	0.460	0.500	115
			0.076	0.039	0.465		
			0.076	0.037	0.458		
			0.076	0.040	0.452		
				0.041	0.468		
f	0.351		0.100	0.055			
			0.083	0.031	0.704	0.760	175
g	0.347	3	0.108	0.061			
			0.086	0.046	0.437	0.530	102
			0.078	0.054	0.435		
			0.075	0.058	0.453		
			0.073	0.061	0.448		
			0.069	0.064	0.452		
h	0.343		0.108	0.061			
			0.086	0.042	0.572	0.680	131
			0.081	0.049	0.567		
			0.078	0.057	0.574		
				0.060	0.576		
l	0.353	5	0.139	0.064			
			0.100	0.049	0.528	0.695	99
			0.092	0.056	0.555		
			0.086	0.062	0.560		
			0.083	0.066	0.593		
				0.069			
k	0.353	3	0.108	0.061			
			0.088	0.044	0.742	0.825	159
			0.083	0.051	0.731		
			0.078	0.053	0.740		
m	0.353	5	0.139	0.064			
			0.083	0.061	0.335	0.540	77
			0.083	0.061	0.379		
			0.080	0.063	0.417		
			0.079	0.064	0.461		
				0.065			
n	0.356		0.139	0.064			
			0.106	0.050	0.719	0.865	123
			0.099	0.051	0.738		
			0.089	0.058	0.744		

Experiment 4

System: Water — Carbon Tetrachloride

Run	Correction factor	Jet No.	Max diam (cm)	Min diam (cm)	Wavelength (cm)	Flowrate (cm^3/sec)	Velocity (cm/sec)
a	0.434	1	0.109	0.061			
			0.072	0.064	0.337	0.530	102
			0.071	0.065	0.346		
				0.066	0.322		
b	0.434		0.109	0.061			
			0.082	0.059	0.372	0.630	122
			0.074	0.068	0.385		
c	0.460	3	0.100	0.061			
			0.072	0.054	0.349	0.540	124
			0.068	0.057	0.381		
d	0.448		0.100	0.061			
			0.067	0.060	0.275	0.470	108
			0.067	0.062	0.304		
				0.063			

Experiment 5

System: Carbon Tetrachloride — Water

Run	Correction factor	Jet No.	Max diam (cm)	Min diam (cm)	Wavelength (cm)	Flowrate (cm^3/sec)	Velocity (cm/sec)
a	0.491	6	0.196	0.066			
			0.126	0.091	0.437	0.574	56
			0.121	0.096	0.478		
				0.104	0.491		
b	0.494		0.196	0.066	0.499		
			0.135	0.105	0.498	0.648	64
			0.129	0.108	0.534		
				0.111	0.593		
d	0.438	1	0.109	0.061			
			0.091	0.052	0.516	0.599	116
			0.090	0.056	0.487		
			0.087	0.062	0.519		
e	0.438		0.109	0.061			
			0.087	0.065	0.350	0.448	86
			0.086	0.067	0.378		
			0.085	0.068	0.360		
				0.069	0.364		
g	0.475	3	0.100	0.061			
			0.076	0.058	0.343	0.418	96
			0.076	0.056	0.373		
			0.075	0.059	0.368		
				0.062	0.356		
k	0.464		0.100	0.061			
			0.088	0.051	0.441	0.500	115
			0.086	0.053	0.445		
			0.085	0.054	0.439		
				0.054			
h	0.462		0.100	0.061			
			0.083	0.038	0.505	0.577	133
			0.081	0.047	0.522		
					0.508		

Experiment 6

System: Water — iso-Amyl Alcohol

Run	Correction factor	Jet No.	Max diam (cm)	Min diam (cm)	Wavelength (cm)	Flowrate (cm^3/sec)	Velocity (cm/sec)
a	0.424	1	0.109	0.061			
			0.086	0.036	0.800	0.485	94
			0.078	0.052	0.802		
				0.063			
b	0.431		0.109	0.061			
			0.086	0.038	1.095	0.600	116
				0.054	1.086		
c	0.433		0.109	0.061			
			0.087	0.043	0.620	0.350	68
			0.076	0.055	0.622		
				0.065	0.619		
d	0.363	5	0.139	0.064			
			0.086	0.034	0.677	0.455	65
			0.076	0.049	0.661		
			0.068	0.057	0.665		
e	0.322		0.139	0.064			
			0.079	0.064	0.801	0.615	87
			0.070	0.054	0.806		
g	0.363		0.139	0.064			
			0.087	0.044	0.693	0.520	74
			0.079	0.053	0.683		
				0.063	0.697		
h	0.409	2	0.100	0.055			
			0.076	0.037	0.634	0.520	120
				0.049			
k	0.418		0.100	0.055			
			0.077	0.038	0.748	0.660	152
			0.069	0.048	0.735		
				0.054			

Experiment 7

System: DIBK — Water

Run	Correction factor	Jet No.	Max diam (cm)	Min diam (cm)	Wavelength (cm)	Flowrate (cm^3/sec)	Velocity (cm/sec)
a	0.394	1	0.109	0.061			
			0.089	0.052	0.554	0.746	114
			0.087	0.060	0.544		
			0.083	0.063	0.559		
b	0.395		0.109	0.061			
			0.094	0.054	0.462	0.667	129
			0.091	0.064	0.462		
			0.090	0.065	0.476		
			0.089	0.066	0.483		
c	0.399		0.109	0.061			
			0.099	0.057	0.663	0.881	170
			0.094	0.065	0.666		
			0.089	0.073	0.670		
d	0.411	2	0.100	0.055			
			0.086	0.052	0.543	0.746	172
			0.079	0.056	0.541		
			0.074	0.060	0.559		
				0.062			
e	0.423		0.100	0.055			
			0.088	0.051	0.720	0.887	204
			0.083	0.055	0.714		
			0.083	0.060	0.715		
f	0.407		0.100	0.055			
			0.081	0.053	0.452	0.633	152
			0.078	0.062	0.479		
			0.075	0.065	0.464		
			0.074	0.067			
g	0.363	5	0.139	0.064			
			0.106	0.064	0.451	0.831	118
			0.092	0.070	0.536		
			0.086	0.074	0.532		
h	0.362		0.139	0.064			
			0.091	0.060	0.398	0.678	96
			0.088	0.069	0.407		
			0.086	0.072	0.430		
k	0.369		0.139	0.064			
			0.103	0.064	0.620		
			0.099	0.065	0.625	0.977	139
				0.069			
l	0.368		0.139	0.064			
			0.091	0.069	0.375	0.729	104
				0.075	0.369		

Experiment 8

System: n-Heptane — Water

Run	Correction factor	Jet No.	Max diam (cm)	Min diam (cm)	Wavelength (cm)	Flowrate (cm^3/sec)	Velocity (cm/sec)
a	0.359	1	0.109	0.061			
			0.094	0.063	0.323	0.645	124
				0.063			
d	0.404	5	0.139	0.064			
			0.128	0.064	0.432	0.781	111
				0.066	0.490		
f	0.335	2	0.100	0.055			
			0.075	0.061	0.272	0.589	135
				0.062			
g	0.333	1	0.109	0.061			
			0.078	0.060	0.258	0.775	150
			0.076	0.064	0.256		
h	0.350		0.109	0.061			
			0.088	0.061	0.383	0.626	121
				0.068			

Experiment 9

System: Cumene — Water

Run	Correction factor	Jet No.	Max diam (cm)	Min diam (cm)	Wavelength (cm)	Flowrate (cm^3/sec)	Velocity (cm/sec)
a	0.335	1	0.109	0.061			
			0.073	0.057	0.239	0.638	123
				0.063	0.249		
b	0.330		0.109	0.061			
			0.081	0.047	0.414	0.796	154
			0.078	0.055	0.419		
				0.058			
c	0.339		0.109	0.061			
			0.080	0.056	0.329	0.512	99
			0.077	0.060	0.323		
			0.074	0.064	0.336		
				0.068	0.332		
d	0.323	2	0.100	0.055			
			0.075	0.048	0.400	0.670	154
			0.075	0.055	0.382		
			0.073	0.058			
e	0.327		0.100	0.055			
			0.069	0.051	0.304	0.561	129
				0.055			
f	0.325		0.100	0.055			
			0.077	0.042	0.502	0.834	192
			0.076	0.053	0.520		
g	0.337	5	0.139	0.064			
			0.096	0.056	0.464	0.823	117
			0.089	0.064	0.486		
			0.085	0.067	0.445		
				0.069			
h	0.335		0.139	0.064			
			0.089	0.067	0.328	0.698	99
			0.085	0.068	0.334		
k	0.337		0.139	0.064			
			0.094	0.061	0.419	0.905	129
			0.092	0.069	0.433		
			0.089	0.074	0.432		

Experiment 10

System: Water — Cumene

Run	Correction factor	Jet No.	Max diam (cm)	Min diam (cm)	Wavelength (cm)	Flowrate (cm^3/sec)	Velocity (cm/sec)
a	0.421	1	0.109	0.061			
			0.086	0.057	0.373	0.645	124
			0.080	0.057	0.378		
			0.076	0.058	0.397		
			0.074	0.059	0.392		
				0.061			
c	0.427		0.109	0.061			
			0.094	0.047	0.587	0.890	172
			0.093	0.056	0.598		
			0.091	0.060	0.594		
b	0.419		0.109	0.061			
			0.093	0.051	0.495	0.770	149
			0.086	0.053	0.496		
			0.084	0.059	0.508		
				0.061	0.503		
d	0.416	2	0.100	0.055			
			0.084	0.043	0.476	0.695	160
			0.081	0.046	0.502		
			0.079	0.048	0.501		
					0.499		
e	0.407		0.100	0.055			
			0.079	0.045	0.529	0.770	177
				0.055	0.531		
f	0.384		0.100	0.055			
			0.078	0.047	0.363	0.605	139
			0.077	0.048	0.369		
			0.075	0.050	0.384		
				0.052			
g	0.419	5	0.139	0.064			
			0.102	0.070	0.532	0.855	121
			0.096	0.075	0.513		
			0.091	0.079	0.534		
h	0.409		0.139	0.064			
			0.105	0.068	0.592	0.990	141
			0.099	0.073	0.612		
			0.094	0.080	0.623		
k	0.403		0.139	0.064			
			0.089	0.077	0.360	0.710	101
			0.088	0.077	0.389		
					0.379		

B. Computer Programs

1. Wave-Length—Interfacial-Tension Relation

The following program was written to solve Eq. (57), to obtain the interfacial tension. It can be separated into three parts: the calling program, the determinant-reduction program, the Bessel-function program.

a. Calling Program ("Valor"). The object of the numeric work is to evaluate a 6×6 complex matrix equation, the matrix being a function of a variable

$$A(\sigma) \circ X = 0 .$$

For nontrival X, $|A(\sigma)| = 0$ must hold, which leads to solving the determinant equation for σ, as it is involved in one row of A only.

$$|A(\sigma)| = \Delta + D\sigma = 0$$

or,

$$\sigma = -\frac{\Delta}{D} .$$

The machine program has as input the raw experimental data, from which it evaluates the program parameters. Then certain values of the Bessel functions $I_1(az)$, $I_2(az)$, $K_1(az)$, $K_2(az)$ are computed; and the matrices (D) and (Δ) are formed. These serve as input to the Gauss-reduction program, which returns the complex determinants D and Δ; the calling program then calculates σ.

VALOR

```
5     READ INPUT TAPE2,1,N,B,A,RE1,RE2,RAT1,RAT2
      BA=B
      B2 = B**2
      Y12 = (B/2.)*(-B+SQRTF(B2+(RE1          )**2))
      Y22 = (B/2.)*(-B+SQRTF(B2+(RE2          )**2))
      X12 = B2 + Y12
      X22 = B2 + Y22
      D1R = SQRTF(X12)
      D1I = SQRTF(Y12)
      D2R = SQRTF(X22)
      D2I = SQRTF(Y22)
      WRITE OUTPUT TAPE3,2,N,B,RE1,RE2,A,RAT1,RAT2
      D1AR = D1R*A
      D1AI = D1I*A
      D2AR = D2R*A
      D2AI = D2I*A
      R1 = SQRTF(D1AR**2+D1AI**2)
      PHI1 = ATANF(D1AI/D1AR)
      R2 = SQRTF(D2AR**2+D2AI**2)
      PHI2 = ATANF(D2AI/D2AR)
      CALL BI(1,BA,0.0,BI1R,BI1I)
      CALL BI(2,BA,0.0,BI2R,BI2I)
      CALL BK(1,BA,0.0,BK1R,BK1I)
      CALL BK(2,BA,0.0,BK2R,BK2I)
      CALL BI(1,R1,PHI1,DI1R,DI1I)
      CALL BI(2,R1,PHI1,DI2R,DI2I)
      CALL BK(1,R2,PHI2,DK1R,DK1I)
      CALL BK(2,R2,PHI2,DK2R,DK2I)
      DI2PR = D1 R*DI1R - D1 I*DI1I -(2./A)*DI2R
      DI2PI = D1 R*DI1I + D1 I*DI1R -(2./A)*DI2I
      DK2PR = -D2 R*DK1R + D2 I*DK1I -(2./A)*DK2R
      DK2PI = -D2 R*DK1I - D2 I*DK1R -(2./A)*DK2I
      DI2PPR=B**2*DI2R
     1   -B*RE1*DI2I
     2     + (6./A**2)*DI2R
     3     - (D1 R/A)*DI1R + (D1 I/A)*DI1I
      DI2PPI=B**2*DI2I
     1   +B*RE1*DI2R
     2     + (6./A**2)*DI2I
     3     -(D1 R/A)*DI1I
     4     - (D1 I/A)*DI1R
      BI2PR = B*BI1R -(2./A)*BI2R
      BI2PI = B*BI1I -(2./A)*BI2I
      BK2PR = -B*BK1R-(2./A)*BK2R
      BK2PI = -B*BK1I-(2./A)*BK2I
      BI2PPR = B**2*BI2R + (6./A**2)*BI2R -(B/A)*BI1R
      BI2PPI = B**2*BI2I + (6./A**2)*BI2I-(B/A)*BI1I
      DK2PPR   =          (B**2+6./A**2)*DK2R
     1  -B*RE2*DK2I
```

VALOR

```
     2          +(D2 R/A)*DK1R
     3          -(D2 I/A)*DK1I
      DK2PPI =              (B**2+6./A**2)*DK2I
     1  +B*RE2*DK2R
     2          +(D2 R/A)*DK1I
     3          +(D2 I/A)*DK1R
      BK2PPR = (B**2+6./A**2)*BK2R  +  (B    /A)*BK1R
      BK2PPI = (B**2+6./A**2)*BK2I  +  (B    /A)*BK1I
      WRITE OUTPUT TAPE3,3,BA,BI1R,BI1I,BK1R,BK1I,BI2R,BI2I,BK2R,BK2I,
     1BI2PR,BI2PI,BK2PR,BK2PI,BI2PPR,BI2PPI,BK2PPR,BK2PPI,
     2D1AR,D1AI,D2AR,D2AI,DI1R,DI1I,DK1R,DK1I,DI2R,DI2I,DK2R,DK2I,
     3DI2PR,DI2PI,DK2PR,DK2PI,DI2PPR,DI2PPI,DK2PPR,DK2PPI
CT
      DIMENSION AR(20,20),AI(20,20),JROW(20),ICOL(20),IROW(20),JCOL(20),
     1          BR(20,20),BM(20,20),AAR(6),AAI(6),CR(20,20),CI(20,20)
      EL = (3.+(A*B)**2)/(A**2*B)
      AR(1,1)=-(2./(RE1*B)   )*BI2PPI-BI2R
      AAR(1)=(EL*BI2PR)/B
      AI(1,1)=(2./(RE1*B)   )*BI2PPR-BI2I
      AAI(1)=(EL*BI2PI)/B
      AR(1,2)=(BK2R+(2./(RE2*B)   )*BK2PPI)*RAT1
      AAR(2)=0.
      AI(1,2)=(BK2I-(2./(RE2*B)   )*BK2PPI)*RAT1
      AAI(2)=0.
      SSQ = (D1R**2+D1I**2)**2
      RED12R=(D1R**2-D1I**2)/SSQ
      RED12I=-2.*D1R*D1I/SSQ
      SSQ = (D2R**2+D2I**2)**2
      RED22R=(D2R**2-D2I**2)/SSQ
      RED22I=-2.*D2R*D2I/SSQ
      AI(1,3)=-(2.*B/RE1 )*(DI2PPR*RED12R                -DI2PPI*RED12I)
      AR(1,3)=(2.*B/RE1 )*(DI2PPI*RED12R+DI2PPR*RED12I)
      AAR(3)=-(EL*B)*(DI2PR*RED12R-DI2PI*RED12I)
      AAI(3)=-(EL*B)*(DI2PR*RED12I+DI2PI*RED12R)
      AAR(4)=0.
      AAI(4)=0.
      AR(1,4)=-(2.*B/RE2 )*(DK2PPI*RED22R+DK2PPR*RED22I)*RAT1
      AI(1,4)=(2.*B/RE2 )*(DK2PPR*RED22R-DK2PPI*RED22I)*RAT1
      AR(1,5)=(2./RE1)*(DI2PR-DI2R/A)/A
      AI(1,5)=(2./RE1)*(DI2PI-DI2I/A)/A
      AAR(5)=EL*DI2I/A
      AAI(5)=-EL*DI2R/A
      AAR(6)=0.
      AAI(6)=0.
      AR(1,6)=(2./(RE2*A))*(DK2R/A-DK2PR)
      AI(1,6)=(2./(RE2*A))*(DK2I/A-DK2PI)
      AR(2,1)=-BI2R
      AI(2,1)=-BI2I
      AR(2,2)=BK2R
      AI(2,2)=BK2I
```

VALOR

```
      AR(2,3)=DI2R
      AI(2,3)=DI2I
      AR(2,4)=-DK2R
      AI(2,4)=-DK2I
      AR(2,5)=0.
      AI(2,5)=0.
      AR(2,6)=0.
      AI(2,6)=0.
      AR(3,1)=-BI2PI/B
      AI(3,1)=BI2PR/B
      AR(3,2)=BK2PI/B
      AI(3,2)=-BK2PR/B
      AR(3,3)=B*(DI2PR*RED12I+DI2PI*RED12R)
      AI(3,3)=-B*(DI2PR*RED12R-DI2PI*RED12I)
      AR(3,4)=-B*(DK2PR*RED22I+DK2PI*RED22R)
      AI(3,4)=B*(DK2PR*RED22R-DK2PI*RED22I)
      AR(3,5)=DI2R/A
      AI(3,5)=DI2I/A
      AR(3,6) = -DK2R/A
      AI(3,6) = -DK2I/A
      AR(4,1)=-(2./(B    *A))*BI2R
      AI(4,1)=-(2./(B    *A))*BI2I
      AR(4,2)=(2./(B    *A))*BK2R
      AI(4,2)=(2./(B    *A))*BK2I
      AR(4,3)=(2.*B/A)*(DI2R*RED12R-DI2I*RED12I)
      AI(4,3)=(2.*B/A)*(DI2R*RED12I+DI2I*RED12R)
      AR(4,4)=-(2.*B/A)*(DK2R*RED22R-DK2I*RED22I)
      AI(4,4)=-(2.*B/A)*(DK2I*RED22R+DK2R*RED22I)
      AR(4,5)=-DI2PI/2.
      AI(4,5)=DI2PR/2.
      AR(4,6)=DK2PI/2.
      AI(4,6)=-DK2PR/2.
      AR(5,1)=-2.*BI2PR
      AI(5,1)=-2.*BI2PI
      AR(5,2)=2.*RAT2*BK2PR
      AI(5,2)=2.*RAT2*BK2PI
      S1R=1.+B**2*RED12R
      S1I=B**2*RED12I
      AR(5,3)=      (S1R*DI2PR-S1I*DI2PI)
      AI(5,3)=      (S1R*DI2PI+S1I*DI2PR)
      S2R=1.+B**2*RED22R
      S2I=B**2*RED22I
      AR(5,4)=-RAT2*(S2R*DK2PR-S2I*DK2PI)
      AI(5,4)=-RAT2*(S2I*DK2PR+S2R*DK2PI)
      AR(5,5)=-      (B/A)*DI2I
      AI(5,5)=      (B/A)*DI2R
      AR(5,6)=RAT2*(B/A)*DK2I
      AI(5,6)=-RAT2*(B/A)*DK2R
      AR(6,1)=(4.      /(B    *A))*(BI2R/A-BI2PR)
      AI(6,1)=(4.      /(B    *A))*(BI2I/A-BI2PI)
```

VALOR

```
      AR(6,2)=-(4.*RAT2/(B    *A))*(BK2R/A-BK2PR)
      AI(6,2)=-(4.*RAT2/(B    *A))*(BK2I/A-BK2PI)
      X=(4.       *B/A)*(DI2PR-DI2R/A)
      Y=(4.       *B/A)*(DI2PI-DI2I/A)
      AR(6,3)=RED12R*X-RED12I*Y
      AI(6,3)=RED12R*Y+RED12I*X
      X=(4.*RAT2*B/A)*(DK2PR-DK2R/A)
      Y=(4.*RAT2*B/A)*(DK2PI-DK2I/A)
      AR(6,4)=-(RED22R*X-RED22I*Y)
      AI(6,4)=-(RED22R*Y+RED22I*X)
      AR(6,5)=-      (DI2PPI/2.-DI2PI/(2.*A)+2.*DI2I/(A**2))
      AI(6,5)=       (DI2PPR/2.-DI2PR/(2.*A)+2.*DI2R/(A**2))
      AR(6,6)=RAT2*(DK2PPI/2.-DK2PI/(2.*A)+2.*DK2I/(A**2))
      AI(6,6)=-RAT2*(DK2PPR/2.-DK2PR/(2.*A)+2.*DK2R/(A**2))
      DO 20I = 1,6
      DO 20J = 1,6
      BR(I,J) = AR(I,J)
 20   BM(I,J) = AI(I,J)
      HOWBIG = SQRTF(DI2PPR**2+DI2PPI**2)
      IF(HOWBIG-.1 E 07)100,100,101
 101  IF(HOWBIG-.1 E 14)102,102,103
 100  SCALE = 1.0
      GO TO 104
 102  SCALE = .1 E-14
      GO TO 104
 103  SCALE = .1 E-20
 104  CALL GAUSS(6,AR,AI,DETR,DETI,SCALE,JROW,ICOL)
      AR(1,1)=AAR(1)
      AI(1,1)=AAI(1)
      AR(1,2)=AAR(2)
      AI(1,2)=AAI(2)
      AR(1,3)=AAR(3)
      AI(1,3)=AAI(3)
      AR(1,4)=AAR(4)
      AI(1,4)=AAI(4)
      AR(1,5)=AAR(5)
      AI(1,5)=AAI(5)
      AR(1,6)=AAR(6)
      AI(1,6)=AAI(6)
      DO 10I=2,6
      DO 10J=1,6
      AR(I,J)=BR(I,J)
 10   AI(I,J)=BM(I,J)
      DO 30I = 1,6
      DO 30J = 1,6
      CR(I,J) = AR(I,J)
 30   CI(I,J) = AI(I,J)
      CALL GAUSS(6,AR,AI,DELR,DELI,SCALE,IROW,JCOL)
      SSQ=DELR**2+DELI**2
      TR=-(DETR*DELR+DETI*DELI)/SSQ
```

VALOR

```
      TI=-(DETI*DELR-DETR*DELI)/SSQ
      VAR=TR*RE1**2
      WRITE OUTPUT TAPE3,4,DETR,DETI,TR,TI,DELR,DELI,VAR
      GO TO 5
1     FORMAT (I2,F8.4,F10.4,2F5.0,2F5.1)
2     FORMAT (21H1INTERFACIAL TENSION.,4X,17HEXPERIMENT NUMBERI3/11H0INP
     1UT DATA/5H0B = F8.4,12X,7HR1    = F5.0,8X,7HR2    = F5.0/5H0A = F8.4
     2,12X,7HRAT1 = F6.4,7X,7HRAT2 = F6.4)
3     FORMAT (1H0//29H BESSEL FUNCTION EVALUATIONS./1H ,15X,4HREAL,9X,9H
     1IMAGINARY,29X,4HREAL,9X,9HIMAGINARY/10H BA       =,E16.8/10H I1(BA)
     2  =2E16.8,10X,9HK1(BA)  =2E16.8/10H I2(BA)  =2E16.8,10X,9HK2(BA)
     3=2E16.8/10H I2P(BA) =2E16.8,10X,9HK2P(BA) =2E16.8/10H I2PP(BA)=2E1
     46.8,10X,9HK2PP(BA)=2E16.8/10H0D1A      =2E16.8,10X,9HD2A      =2E16.
     58/10H I1(DA)  =2E16.8,10X,9HK1(DA)  =2E16.8/10H I2(DA)  =2E16.8,10
     6X,9HK2(DA)  =2E16.8/10H I2P(DA) =2E16.8,10X,9HK2P(DA) =2E16.8/10H
     7I2PP(DA)=2E16.8,10X,9HK2PP(DA)=2E16.8)
4     FORMAT (1H0///1H ,51X,9HD        =2E16.8/10H0      T  =2E16.8/1H0,51
     1X,9HDELTA    =2E16.8/1H0,F10.0)
      END(1,1,0,0,0,0,1,0,0,0,0,0,0,0,0)
```

b. Gauss-Reduction Program. The Gauss-reduction method is used to evaluate a determinant with complex values. All complex arithmetic is written out explicitly in Fortran language, rather than through the use of the "complex arithmetic facility" now provided on library tapes for the IBM 7090. This allows for extension later to double-precision arithmetic via the applicable library programs. Therefore, the resulting program may be used either in single precision for increased speed; or in double precision for control of cumulative round-off error, which is often a problem in matrix and determinant operations.

Upon entry to the program, a search is made among the n^2 elements of the matrix for the element $z = x + iy$ such that $x^2 + y^2$ is maximum. By interchanging rows and columns, this element is placed in the pivot position a_{11}, changing the sign of the determinant if applicable. Following this, the remaining rows are transformed as follows:

$$\left.\begin{aligned} a_{ij} &\Leftarrow a_{ij} - a_{i1}\frac{a_{1j}}{a_{11}} \\ a_{i1} &\Leftarrow 0 \end{aligned}\right\} \begin{aligned} i &= 2, \cdots, n \\ j &= 1, \cdots, n, \end{aligned}$$

(where $\Leftarrow$ means "is replaced by").

Now a_{22} becomes the pivot element, into which position is moved the maximal element in the remaining $(n-1) \times (n-1)$ matrix. The second and all following steps in the reduction are accomplished exactly as above:

$$\left.\begin{aligned} a_{ij} &\Leftarrow a_{ij} - a_{ik}\frac{a_{kj}}{a_{kk}} \\ a_{ik} &\Leftarrow 0 \end{aligned}\right\} \begin{aligned} k &= 2, \cdots, n \\ i &= k+1, \cdots, n \\ j &= 2, \cdots, n. \end{aligned}$$

There results a matrix that is zero everywhere below the principal diagonal. The determinant of this matrix is simply

$$D = \prod_{i=1} a_{ii} .$$

Inasmuch as the elements of this diagonal may be very large or very small, overflow or underflow may take place in the formation of the product. For control of this condition, provision is made to supply the program with a scale factor used as follows: The initial value of D is $D = (\text{scale factor}) \times 1$, and subsequently $D \Leftarrow a_{ii} \times D$, $i = 1, \cdots, n$. Then if overflow is likely to occur, the scale factor can be set to some suitable small number. If at any stage of the reduction the pivot element is zero, then the determinant is set to zero, and control is returned to the main program. The program is written so that it may be extended easily to solve a set of nonhomogeneous equations with complex coefficients,

$$Az = b ,$$

where A is $n \times n$, $n \leq 20$.

In the calling program, we define in a dimension statement a floating-point variable AR(20, 20) for the real part of the matrix and AI(20, 20) for the imaginary part. Then, after selecting a suitable scale factor, the subroutine is called in this manner:

CALL GAUSS(N, AR, AI, SCALE, DR, DI).

Upon return, DR and DI will contain the real and imaginary parts of the determinant, respectively.

The program was checked by using numeric examples of Vandermonde's determinant, which may be solved easily for comparison with the result of the reduction:

$$v = \begin{vmatrix} 1 & z_1 & z_1^2 \cdots z_1^{n-1} \\ 1 & z_2 & \\ \vdots & & \\ 1 & z_n \cdots & \cdots z_n^{n-1} \end{vmatrix} .$$

Then, as may be verified easily,

$$v = (z_n - z_{n-1})(z_n - z_{n-2})\cdots(z_n - z_1) \times$$

$$(z_{n-1} - z_{n-2})(z_{n-1} - z_{n-3})\cdots(z_{n-1} - z_1) \times$$

$$(z_3 - z_2)(z_3 - z_1) \times (z_2 - z_1).$$

The single-precision program in the 6×6 case yielded five significant figures with an error whose absolute value was less than 1 in the last place, while the double-precision program gave eight significant figures.

```
CGAUSS
      SUBROUTINE GAUSS(M,BR,BI,DETR,DETI,FACTOR,JROW,ICOL)
D     DIMENSIONAR(20,20),AI(20,20),JROW(20),ICOL(20),BR(20,20),BI(20,20)
      N = M
      DO 33 I=1,N
      DO 33 J=1,N
D     AR(I,J)=BR(I,J)
D  33 AI(I,J)=BI(I,J)
D     SCALE = FACTOR
      DO 11 IT = 1,N
      JROW(IT) = IT
11    ICOL(IT) = IT
      DO 4 L = 1,N
      K = L+1
D     AMAX = 0.
      DO 20 J = L,N
      DO 20 I = L,N
D     SSQ = AR(J,I)**2 + AI(J,I)**2
D     IF(AMAX-SSQ) 10,20,20
10    JR = J
      IR = I
D     AMAX = SSQ
20    CONTINUE
D     SSQ = AMAX
D     IF(SSQ) 21,100,21
21    IF(JR-L) 30,40,30
30    DO 31 I = 1,N
D     CR = AR(JR,I)
D     CI = AI(JR,I)
D     AR(JR,I) = AR(L,I)
D     AI(JR,I) = AI(L,I)
D     AR(L,I) = CR
D31   AI(L,I) = CI
D     SCALE = -SCALE
      JRO = JROW(JR)
      JROW(JR) = JROW(L)
      JROW(L) = JRO
40    IF(IR-L) 60,50,60
60    DO 61 J = 1,N
D     CR = AR(J,IR)
D     CI = AI(J,IR)
D     AR(J,IR) = AR(J,L)
D     AI(J,IR) = AI(J,L)
D     AR(J,L) = CR
D61   AI(J,L) = CI
D     SCALE = -SCALE
      ICO = ICOL(IR)
      ICOL(IR) = ICOL(L)
      ICOL(L) = ICO
50    DO 4 I = K,N
D2    SQ = AR(I,L)**2 +AI(I,L)**2
D     IF(SQ) 3,4,3
3     DO 14 JJ = L,N
      J = N+L-JJ
D     AX = AR(I,J)-(AR(I,L)*AR(L,J)*AR(L,L)+AR(I,L)*AI(L,J)*AI(L,L)
D    1    +AI(I,L)*AR(L,J)*AI(L,L)-AI(I,L)*AI(L,J)*AR(L,L))/SSQ
D     AI(I,J) = AI(I,J)-(AI(I,L)*AI(L,J)*AI(L,L)+AI(I,L)*AR(L,J)*AR(L,L)

D    1          +AR(I,L)*AI(L,J)*AR(L,L)-AR(I,L)*AR(L,J)*AI(L,L))/SSQ
D14   AR(I,J) = AX
4     CONTINUE
D     IF(SCALE) 7,9,7
D9    SCALE = 1.
D7    DETR = SCALE
D     DETI = 0.
      DO 5 I = 1,N
D     DR = DETR
D     DETR = DETR*AR(I,I)-DETI*AI(I,I)
D5    DETI = DETI*AR(I,I)+DR*AI(I,I)
8     RETURN
D100  DETR = 0.
D     DETI = 0.
      RETURN
      END
```

c. Bessel-Function Program

None of the existing programs covered a sufficiently wide range of values of the complex arguments to be useful in the present situation. In the same manner as the National Bureau of Standards,[34,35] we used the regular Bessel-function series and truncated the summation after the first 26 terms. We calculated $J_n(z)$ and $Y_n(z)$ from the series, and then the modified Bessel functions $I_n(z)$ and $K_n(z)$ from combinations of $J_n(z)$ and $Y_n(z)$.

The program's accuracy was checked by using the previously mentioned tables from the National Bureau of Standards. Using single-precision arithmetic, we obtained values whose cumulative round-off error was less than 26 in the eighth place. If the double-precision-arithmetic facility of the IBM 7090 was used, this error was cut to 1 in the eighth place.

To use the program the CALL statements are written as follows:

```
CALL   BJ(N, X, Y, BJR, BJI)
CALL   BY(         BYR,BYI)
CALL   BI (                )
CALL   BK(                 )
```

where $z = X + iY$. On return, the real part of $J_n(z)$ will be in BJR and the imaginary part in BJI. Corresponding statements hold for $Y_n(z)$, $I_n(z)$, and $K_n(z)$.

```
CBJ
      SUBROUTINE BJ(N,RHO,PHI,SUMR,SUMI)
      XN=N
      R=RHO/2.0
      RSQ=(RHO/2.0)**2
      FP=R**XN/FACN (XN)
      SUMR=FP*COSF(XN*PHI)
      SUMI=FP*SINF(XN*PHI)
      DO 1 K=1,26
      XK=K
      FA=-(RSQ/(XK*(XK+XN)))*FP
      FP=FA
      SUMR=FA*COSF((2.0*XK+XN)*PHI)+SUMR
    1 SUMI=FA*SINF((2.0*XK+XN)*PHI)+SUMI
      RETURN
      END
CBY
      SUBROUTINE BY(N,RHO,PHI,SUMR,SUMI)
      PI=3.141592654
      FIRSTR=0.0
      FIRSTI=0.0
      XN=N
      R=RHO/2.0
      RSQ=R**2
      IF(N-1)3,1,1
    1 FP=FACN (XN-1.0)/(R**XN)
      SUMR=FP*COSF(XN*PHI)
      SUMI=-FP*SINF(XN*PHI)
      IF(N-1) 6,6,5
5     M=N-1
      DO 2K=1,M
      XK=K
      FA=(RSQ/((XN-XK)*XK))*FP
      FP=FA
      SUMR=FA*COSF(PHI*(2.0*XK-XN))+SUMR
    2 SUMI=FA*SINF(PHI*(2.0*XK-XN))+SUMI
6     FIRSTR=-SUMR/PI
      FIRSTI=-SUMI/PI
    3 X=LOGF(R)+0.577215665
      Y=PHI
      CALL BJ(N,RHO,PHI,SUMR,SUMI)
      TWOR=2.0*(X*SUMR-Y*SUMI)/PI
      TWOI=2.0*(X*SUMI+Y*SUMR)/PI
      FP = -(R**XN)/FACN(XN)
      FR=FP*PHY (XN,0.0)
      SOMMER=FR*COSF(XN*PHI)
      SOMMEI=FR*SINF(XN*PHI)
      DO 4 K=1,26
      XK=K
      FA=-(RSQ/(XK*(XN+XK)))*FP
      FP=FA
      FA=FA*PHY (XN,XK)

      SOMMER=FA*COSF(PHI*(2.0*XK+XN))+SOMMER
    4 SOMMEI=FA*SINF(PHI*(2.0*XK+XN))+SOMMEI
      SOMMER=SOMMER/PI
      SOMMEI=SOMMEI/PI
      SUMR=FIRSTR+TWOR+SOMMER
      SUMI=FIRSTI+TWOI+SOMMEI
      RETURN
      END
```

```
CBI
      SUBROUTINE BI(N,RHO,PHI,BRI,BII)
      PI = 3.141592654
      XN=N
      PHO = PHI + PI/2.0
      CALL BJ(N,RHO,PHO,BRJ,BIJ)
      X=COSF(XN*PI/2.0)
      Y=-SINF(XN*PI/2.0)
      BRI = X*BRJ - Y*BIJ
      BII = X*BIJ + Y*BRJ
      RETURN
      END
CBK
      SUBROUTINE BK(N,RHO,PHI,BRK,BIK)
      PI=3.141592654
      PHO=PHI+PI/2.0
      XN=N
      CALL BJ(N,RHO,PHO,BRJ,BIJ)
      CALL BY(N,RHO,PHO,BRY,BIY)
      X=(PI/2.0)*COSF((XN+1.0)*PI/2.0)
      Y=(PI/2.0)*SINF((XN+1.0)*PI/2.0)
      BRK=X*(BRJ-BIY)-(Y*(BIJ+BRY))
      BIK=X*(BIJ+BRY)+Y*(BRJ-BIY)
      RETURN
      END
CPHY
      FUNCTION PHY (XN,XK)
      SUM=0.0
      IF(XN-1.0) 3,1,1
    1 N=XN
      DO 2I=1,N
      XI=I
    2 SUM=1.0/(XK+XI)+SUM
    3 IF(XK-1.0) 4,5,5
    4 PHY=SUM
      RETURN

    5 K=XK
      SOMME=0.0
      DO 6 I=1,K
      XI = I
    6 SOMME=1.0/XI+SOMME
      PHY=2.0*SOMME+SUM
      RETURN
      END
CFACN
      FUNCTION FACN (XN)
      IF(XN-2.0) 1,2,3
    1 FACN= 1.0
      RETURN
    2 FACN=2.0
      RETURN
    3 N=XN
      FACN=2.0
      DO 4 I=3,N
      XI=I
    4 FACN=FACN*XI
      RETURN
      END
```

2. Velocity Profile — Schlicting Approach

This program is a straightforward calculation of the velocity profile from Eqs. (76) through (79). A second program is needed to check whether it is necessary to use Eq. (82) for the momentum balance, or whether it may be approximated by Eq. (85). The second program calculates the second integral of Eq. (82) with Simpson's rule.

```
CCYP
*       XEQ
        DIMENSION  X(7),A(7),AA(7),HL3(7),HL31(7),GL2(7),G(7),HL2(7),B(7),
       2HL2R(7)
   27   READ INPUT TAPE  2,7,(X(I),I=1,7),RHO1,RHO2,HMU1,HMU2,US,AS,RUN
    7   FORMAT (7F5.0,2F5.3,2F6.4,F5.0,F6.4,F4.0)
        R1=(US*AS*RHO1)/HMU1
        R2=(US*AS*RHO2)/HMU2
        X0=R1/4.0
        WRITE OUTPUT TAPE 3,4,R1,R2,X0
    4   FORMAT (1H0,3F10.2)
    9   DO 10 I=1,7
   10   AA(I)=16.0/R1
        DO 1 I=1,7
    1   A(I)=((AA(I)*X(I)**2)/(8.0*X(I)-R1))**0.5
   12   DO 16 I=1,7
        HL3(I)=(AA(I)*X(I)**2+R1*A(I)**2)
        HL31(I)=(AA(I)*X(I)**2+R2*A(I)**2)
        GL2(I)=((2.0*R2*A(I)**2)/HL3(I))-1.0
        G(I)=(((4.0*R2*A(I)**2)*((HL31(I)/HL3(I))-1.0)/HL3(I))+1.0)**0.5
        HL2(I)=GL2(I)/G(I)
        B(I)=((1.0-HL2(I))/(1.0+HL2(I)))*(R2*A(I)**2/X(I)**2)**G(I)
   16   CONTINUE
   90   FORMAT(1H0,7E14.6)
        WRITE OUTPUT TAPE 3,90,(G(J),J=1,7)
        WRITE OUTPUT TAPE 3,90,(B(J),J=1,7)
        DO22 I=1,7
        DO 20 L=11,25,2
        R=FLOATF(L-1)*0.1*A(I)
        HL2R(I)=(1.0-B(I)*(X(I)**2/(R2*R**2))**G(I))/(1.0+B(I)*(X(I)**2/
       2(R2*R**2))**G(I))
        UE    =((2.0*X(I))/R2)*((G(I)/R)**2)*(1.0-HL2R(I)**2)
        VE    =(2.0/(R*R2))*((G(I)**2)*(1.0-HL2R(I)**2)-(1.0+G(I)*HL2R(I)))
        WRITE OUTPUT TAPE 3,21,RUN,UE,VE,R,I
   20   CONTINUE
   21   FORMAT(1H0,F4.1,3X,2F12.4,3X,F7.4,3X,I3)
   22   CONTINUE
        DO26 I=1,7
        DO 24 L=1,11,2
        R=FLOATF(L-1)*0.1*A(I)
        UI    =(8.0*AA(I)*X(I)**3.0)/((R1*R**2+AA(I)*X(I)**2)**2)
        VI    =(4.0*R*(AA(I)*X(I)**2-R1*R**2))/((AA(I)*X(I)**2+R1*R**2)**2)
        WRITE OUTPUT TAPE 3,21,RUN,UI,VI,R,I
   24   CONTINUE
   26   CONTINUE
        GO TO 27
        END
*       DATA
```

3. Velocity Profile — Exponential Approach

The following program is again a straightforward calculation of the velocity profile. However, a trial-and-error solution of Eq. (92) is necessary before the velocity can be calculated. After this is done, the profiles are calculated from Eq. (90) and (91).

CY2

```
      DIMENSION  X(7)
   10 READ INPUT TAPE  2,7,(X(I),I=1,7),RHO1,RHO2,HMU1,HMU2,US,AS,RUN
    7 FORMAT (7F5.0,2F5.3,2F6.4,F5.0,F6.4,F4.0)
      R1=(US*AS*RHO1)/HMU1
      R2=(US*AS*RHO2)/HMU2
      A=(RHO2*HMU2)/(RHO1*HMU1)
      WRITE OUTPUT TAPE 3,24,R1,R2,A
   24 FORMAT(1H0,2F8.2,F8.4)
      DO 20I=1,7
      PB=10.000
      PS=0.000
    5 P=(PB+PS)/2.0
      D=(3.0/P)*EXPF(-P*X(I)/R1)*(1.0-(1.0-P/4.0)**2*(1.0-A))
      D=D-1.000
      IF(D) 11,12,14
   11 PB=P
      D=-1.0*D
      GO TO 15
   14 PS=P
   15 IF(D-0.002) 12,12,5
   12 B1=(P/(2.0      ))*EXPF(-P*X(I)/R1)
      B2=(HMU1/HMU2)*B1
      AA=(LOGF(1.0-P/4.0)/(-B1      ))**0.5
      AAA=EXPF(-P*X(I)/R1-AA**2*      (B1-B2)) *2.0
      DO 30 L=1,11,2
      R=FLOATF(L-1)*0.1*AA
      UI=2.0*EXPF(-P*X(I)/R1-B1*R**2)
      WRITE OUTPUT TAPE 3,21,RUN,UI,R
   30 CONTINUE
      DO 40 L=11,31,2
      R=FLOATF(L-1)*0.1*AA
      UE=AAA*                          EXPF(-B2*R**2)
      WRITE OUTPUT TAPE 3,21,RUN,UE,R
   40 CONTINUE
      UAV=(2.0*EXPF(-P*X(I)/R1))*(1.0-EXPF(-B1*AA**2))/(B1*AA**2)
      WRITE OUTPUT TAPE 3,23,P,B1,AA,AAA,UAV
   21 FORMAT(1H0,F5.1,F12.4,3X,F7.4)
   23 FORMAT(1H0,5F12.4)
   20 CONTINUE
      GO TO 10
      END(1,1,0,0,0,0,1,0,0,0,0,0,0,0,0)
```

REFERENCES

1. C. C. Addison, Phil. Mag. 36, 73 (1945).
2. C. C. Addison, J. Chem. Soc. 535 (1943).
3. Ibid., 252 (1944).
4. Ibid., 477 (1944).
5. Ibid., 98 (1945).
6. Ibid., 354 (1945).
7. Giorgio Bidone, Expériences sur la Forme et la Direction des Veines et des Courants d'Eau Lancés par Diverses Ouvertures, 1829; Torino, Mémoires de l'Académie Royale des Sciences de Turin 34, 229 (1830).
8. G. Birkhoff and E. H. Zarantonello, Jets, Wakes, and Cavities, (Academic Press, Inc., New York, 1957), pp. 270-279.
9. N. Bohr, Phil. Trans. A207, 341 (1908-1909).
10. W. N. Bond and H. O. Puls, Phil. Mag. (7) 24, 864 (1937).
11. E. J. Burcik, J. Colloid Sci. 5, 421 (1950).
12. Ibid., 6, 522 (1951).
13. Ibid., 8, 520 (1953).
14. S. Chandrasekhar, Hydrodynamic and Hydromagnetic Stability, (Clarendon Press, London, 1961), pp. 515-540.
15. Harold T. Davis, Introduction to Nonlinear Differential and Integral Equations, (U. S. Government Printing Office, Washington, D. C., 1960), pp. 57-65.
16. R. Defay and J. R. Hommelen, J. Colloid Sci. 13, 553 (1958).
17. Ibid., 14, 401 (1959).
18. Ibid., 14, 411 (1959).
19. P. H. Garner and P. Mina, Trans. Faraday Soc. 55, 1607 (1959).
20. R. S. Hansen, M. E. Purchase, T. C. Wallace, and R. W. Woody, J. Phys. Chem. 62, 210 (1958).
21. R. S. Hansen and T. C. Wallace, J. Phys. Chem. 63, 1085 (1959).
22. R. S. Hansen, J. Phys. Chem. 64, 637 (1960).
23. R. S. Hansen, J. Colloid Sci. 16, 549 (1961).
24. P. Magnus, Poggendorff's Annalen der Physik 25 (1855).

25. H. S. Mickley, T. K. Sherwood, and C. E. Reed, Applied Mathematics in Chemical Engineering (McGraw-Hill Book Co., Inc., New York, 1957), 2nd. ed., pp. 170-180.

26. J. Okabe, Reps. Res. Inst. Fluid Eng., Kyushu University 5, No. 1, 1 (1948).

27. P. O. Pedersen, Phil. Trans. A207, 341 (1906-1907).

28. Lord Rayleigh, Proc. Roy. Soc. (London) 29, 71 (1879).

29. H. Schlicting, Boundary Layer Theory (McGraw-Hill Book Co., Inc., New York, 1955), 1st ed., pp. 159-162.

30. H. Schlicting, ibid., pp. 201-213.

31. H. Stocker, Z. physik Chem. 94, 149 (1920).

32. K. L. Sutherland, Rev. Pure and Appl. Chem. 1, 35 (1951).

33. K. L. Sutherland, Australian J. Chem. (7) 4, 319 (1954).

34. Table of the Bessel Functions $J_0(z)$ and $J_1(z)$ for Complex Arguments (Columbia University Press, New York, 1947), 2nd ed.

35. Tables of the Bessel Functions $Y_0(z)$ and $Y_1(z)$ for Complex Arguments (Columbia University Press, New York, 1950).

36. W. D. E. Thomas and L. Potter, in Proceedings of the Third World Congress on Surface Active Agents, Cologne, September 1960 (Universitatsdruckerei, Mainz, Germany, 1961).

37. S. Tomotika, Proc. Roy. Soc. (London) A150, 322 (1935).

38. C. R. Wylie, Advanced Engineering Mathematics (McGraw-Hill Book Co., Inc., New York, 1951), pp. 249-287.

This report was prepared as an account of Government sponsored work. Neither the United States, nor the Commission, nor any person acting on behalf of the Commission:

A. Makes any warranty or representation, expressed or implied, with respect to the accuracy, completeness, or usefulness of the information contained in this report, or that the use of any information, apparatus, method, or process disclosed in this report may not infringe privately owned rights; or

B. Assumes any liabilities with respect to the use of, or for damages resulting from the use of any information, apparatus, method, or process disclosed in this report.

As used in the above, "person acting on behalf of the Commission" includes any employee or contractor of the Commission, or employee of such contractor, to the extent that such employee or contractor of the Commission, or employee of such contractor prepares, disseminates, or provides access to, any information pursuant to his employment or contract with the Commission, or his employment with such contractor.